

1 **Multiple pathways for the formation of secondary organic aerosol in North China Plain**  
2 **in summer**

3 Yifang Gu<sup>1,4</sup>, Ru-Jin Huang<sup>1,2,3,4</sup>, Jing Duan<sup>1</sup>, Wei Xu<sup>1</sup>, Chunshui Lin<sup>1</sup>, Haobin Zhong<sup>1,4</sup>, Ying  
4 Wang<sup>1</sup>, Haiyan Ni<sup>1</sup>, Quan Liu<sup>5</sup>, Ruiguang Xu<sup>6,7</sup>, Litao Wang<sup>6,7</sup>, Yong Jie Li<sup>8</sup>

5 <sup>1</sup>SKLLQG, Center for Excellence in Quaternary Science and Global Change, Institute of Earth  
6 Environment, Chinese Academy of Sciences, Xi'an 710061, China

7 <sup>2</sup>Open Studio for Oceanic-Continental Climate and Environment Changes, Pilot National  
8 Laboratory for Marine Science and Technology (Qingdao), Qingdao 266000, China

9 <sup>3</sup>Institute of Global Environmental Change, Xi'an Jiaotong University, Xi'an 710049, China

10 <sup>4</sup>University of Chinese Academy of Sciences, Beijing 100049, China

11 <sup>5</sup>State Key Laboratory of Severe Weather & Key Laboratory of Atmospheric Chemistry of C  
12 MA, Chinese Academy of Meteorological Sciences, Beijing 100081, China

13 <sup>6</sup>Department of Environmental Engineering, School of Energy and Environmental Engineering,  
14 Hebei University of Engineering, Handan 056038, China

15 <sup>7</sup>Hebei Key Laboratory of Air Pollution Cause and Impact, Handan 056038, China

16 <sup>8</sup>Department of Civil and Environmental Engineering, and Centre for Regional Oceans, Faculty  
17 of Science and Technology, University of Macau, Taipa, Macau 999078, China

18 *Correspondence to:* Ru-Jin Huang ([rujin.huang@ieccas.cn](mailto:rujin.huang@ieccas.cn))

19

20

21 **Abstract**

22 Secondary organic aerosol (SOA) has been identified as a major contributor to fine  
23 particulate matter (PM<sub>2.5</sub>) in North China Plain (NCP). However, the chemical mechanisms  
24 involved are still unclear due to incomplete understanding of its multiple formation processes.  
25 Here we report field observations in summer in Handan of NCP, based on high-resolution  
26 online measurements. Our results reveal the formation of SOA via photochemistry and two  
27 types of aqueous-phase chemistry, the latter of which include nocturnal and daytime processing.  
28 The photochemical pathway is the most important under high O<sub>x</sub> (=O<sub>3</sub> + NO<sub>2</sub>) conditions (65.1  
29 ± 20.4 ppb). The efficient SOA formation from photochemistry (~~photochem-SOA~~O<sub>x</sub>-initiated-  
30 SOA) dominated the daytime (65% to OA) with an average growth rate of 0.8 μg m<sup>-3</sup> h<sup>-1</sup>.  
31 During the high relative humidity (RH: 83.7 ± 12.5 %) period, strong nocturnal aqueous-phase  
32 SOA formation (aq-SOA) played a significant role in SOA production (45% to OA) with a  
33 nighttime growth rate of 0.6 μg m<sup>-3</sup> h<sup>-1</sup>. Meanwhile, an equally fast growth rate of 0.6 μg m<sup>-3</sup> h<sup>-1</sup>  
34 <sup>1</sup> of ~~photochem-SOA~~O<sub>x</sub>-initiated-SOA from daytime aqueous-phase photochemistry was also  
35 observed, which contributed 39% to OA, showing that photochemistry in the aqueous phase is  
36 also a non-negligible pathway in summer. The primary-related-SOA (SOA attributed to  
37 primary particulate organics) and aq-SOA are related to residential coal combustion activities,  
38 supported by distinct fragments from polycyclic aromatic hydrocarbons (PAHs). Moreover, the  
39 conversion and rapid oxidation of primary-related-SOA to aq-SOA could be possible in the  
40 aqueous phase under high-RH conditions. This work sheds light on the multiple formation  
41 pathways of SOA in ambient air of complex pollution, and improves our understanding of  
42 ambient SOA formation and aging in summer with high oxidation capacity.

43

44 **KEYWORDS:** secondary organic aerosol, aqueous-phase chemistry, photochemistry, multiple-  
45 phase chemistry, complex air pollution

46

## 47 1. Introduction

48 Rapid economic growth and urbanization processes have led to severe particulate air  
49 pollution in China, affecting air quality, climates and human health (Huang et al., 2014;  
50 Cohen et al., 2017; An et al., 2019). Organic aerosol (OA) is a major component of aerosol  
51 particles, consisting of 20-90% of fine particle mass (Jimenez et al., 2009; Zhang et al., 2011).  
52 OA is either emitted directly from primary sources (referred to as primary OA, POA) such as  
53 traffic, cooking, coal combustion, and biomass burning, or produced through gas-to-particle  
54 conversion (referred to as secondary OA, SOA) in the atmosphere. In recent years, with the  
55 implementation of control measures, the POA fraction is decreasing and SOA fraction is  
56 increasing in North China Plain (NCP), indicating that SOA is becoming more critical for urban  
57 air quality (Huang et al., 2019; Xu et al., 2019; Gu et al., 2020). However, our understanding  
58 of the formation mechanisms and evolution processes of SOA is still limited.

59 Generally, SOA can be formed through gas-phase photochemical oxidation of volatile  
60 organic compounds (VOCs) followed by nucleation or condensation of oxidation products onto  
61 the preexisting particles (Donahue et al., 2006). Herndon et al., (2008) showed that oxygenated  
62 organic aerosol (OOA), a surrogate of SOA, was well correlated with odd oxygen ( $O_x = O_3 +$   
63 nitrogen dioxide ( $NO_2$ )) during photochemical processing. SOA can also be formed in the  
64 aqueous phase on wet aerosols, clouds and fogs through further chemical processes of water-  
65 soluble organic compounds or organic products of gas-phase photochemistry (Ervens et al.,  
66 2011, 2014). A growing number of laboratory studies and field measurements have indicated  
67 that aqueous-phase processes contribute efficiently to the formation of SOA (Gilardoni et al.,  
68 2016; Bikkina et al., 2017). However, how photochemistry and aqueous-phase chemistry  
69 coordinate to affect the formation of SOA is still unclear, despite numerous measurements to  
70 explore this question using aerosol chemical speciation monitor (ACSM) or aerosol mass  
71 spectrometer (AMS) (Hu et al., 2016b; Hu et al., 2017; Sun et al., 2016; Li et al., 2017; Sun et  
72 al., 2018b; Huang et al., 2019; Gu et al. 2020; Kuang et al., 2020). Field measurements in  
73 Beijing suggested that gas-phase photochemical oxidation can play a dominant role in SOA  
74 formation (Sun et al., 2016; Hu et al., 2016a). Xu et al., (2017) showed that less oxidized-  
75 OOA (LO-OOA) was mainly formed through photochemical oxidation, while the more oxidized-  
76 OOA (MO-OOA) formation was dominantly formed by aqueous-phase chemistry in Beijing  
77 for different seasons. Kuang et al. (2020) investigated the effects of gas-phase and aqueous-  
78 phase photochemical processes on the formation of SOA and found that photochemical  
79 aqueous-phase SOA formation dominantly contributed to daytime OOA formation in winter  
80 Gucheng, located between Beijing (~100 km) and Baoding (~40 km) on the NCP. We found  
81 that photochemical processing attributed mostly to MO-OOA in summertime Beijing (Gu et al.,  
82 2020). Although these studies provided important insights into SOA formation processes, our  
83 understanding on the photochemical and aqueous-phase formation pathways for SOA and their

84 impacts on oxidation degree are far from complete. This lack of understanding is especially so  
85 under the conditions that atmospheric oxidative capacity and pollution characteristics have been  
86 largely changing in China due to large reduction in direct emissions of air pollutants.

87 In this study, we investigated the photochemical versus aqueous-phase processing for SOA  
88 composition and oxidation degree of OA in summertime Handan, which is a typical  
89 industrialized city in the NCP region. The city is located at the intersectional area of Hebei,  
90 Shanxi, Henan, and Shandong—four heavily urbanized and industrialized provinces (Fig. S1),  
91 and it is therefore an ideal site to investigate the SOA formation pathways in the NCP region.  
92 The multiple formation pathways, evolution of SOA composition, and oxidation degree under  
93 different meteorological conditions were discussed, which sheds light on the aqueous-phase  
94 chemistry and photochemical processing in SOA formation in the NCP region of China.

## 95 **2. Experimental methods**

### 96 **2.1 Sampling site**

97 Measurements were conducted from 10<sup>th</sup> August 2019 to 17<sup>th</sup> September 2019 on the campus  
98 of Hebei University of Engineering (36.57 N, 114.50 E), located at the southeast edge of urban  
99 Handan (Fig. S1). The site is surrounded by a school and residential areas, ~300 m north to  
100 South Ring Road and ~400 m northeast to the Handan Highway (S313). The sampling site is  
101 on the rooftop of a four-floor building, approximately 12 m above the ground.

### 102 **2.2 Instrumentation**

103 Real-time non-refractory PM<sub>2.5</sub> composition was measured by a soot particle long time-of-  
104 flight aerosol mass spectrometer (SP-LToF-AMS, Aerodyne Research Inc.) with a time  
105 resolution of 1 min. The detailed instrument description and operation of AMS were reported  
106 in Onasch et al., (2012). Compared to the conventional AMS, the LToF mass analyzer can  
107 provide much better mass resolution of ~8000. During the campaign, the instrument was  
108 operated in the “laser off” mode and only the standard tungsten vaporizer was applied.  
109 Therefore, only non-refractory PM<sub>2.5</sub> components (NR-PM<sub>2.5</sub>) were measured, including  
110 organics (Org), nitrate (NO<sub>3</sub>), sulfate (SO<sub>4</sub>), ammonium (NH<sub>4</sub>), and chloride (Chl). Ambient  
111 air was sampled and dried by a Nafion dryer (MD-700-24S, Perma Pure, Inc.) at a flow rate of  
112 5 L min<sup>-1</sup>, and then sub-sampled into the SP-LToF-AMS at a flow rate of ~ 0.1 L min<sup>-1</sup>. An  
113 aerodynamic PM<sub>2.5</sub> lens was used to focus the particle into a beam, which was then impacted  
114 on the heated tungsten surface (~ 600 °C) and flash-vaporized. Electron ionization with 70 eV  
115 was used to ionize the vaporized gases. The ionization efficiency (IE) and the relative ionization  
116 efficiency (RIE) calibrations (Jimenez et al., 2003) were conducted by using 350 nm  
117 ammonium nitrate (NH<sub>4</sub>NO<sub>3</sub>) and ammonium sulfate ((NH<sub>4</sub>)<sub>2</sub>SO<sub>4</sub>) particles.

118 Gaseous pollutants including SO<sub>2</sub> (9850 SO<sub>2</sub> analyzer, Ecotech), NO<sub>2</sub> (Model 42i NO-NO<sub>2</sub>-  
119 NO<sub>x</sub> analyzer, Thermo Scientific), CO (Model 48i carbon monoxide analyzer, Thermo  
120 Scientific), O<sub>3</sub> (Model 49i ozone analyzer, Thermo Scientific), and meteorological parameters  
121 including RH and temperature were also measured during the observation period. Furthermore,  
122 an aethalometer (Model AE-33, Magee Scientific) was deployed to measure the mass  
123 concentration of black carbon (BC) at a time resolution of 1 min.

### 124 **2.3 Data Analysis**

125 The data analysis software (SQUIRREL, version 1.63I and PIKA, 1.23I) within Igor Pro 6.37  
126 (WaveMetrics) was used to analyze the AMS data. The experimental RIE values of 4 (NH<sub>4</sub>)  
127 and 1.2 (SO<sub>4</sub>) and the standard RIE values of 1.4 (Org), 1.1 (NO<sub>3</sub>) and 1.3 (Chl) were used.  
128 The composition-dependent collection efficiency (CDCE, Middlebrook et al., 2012) was used  
129 to compensate for the incomplete detection caused by particle bounce on the vaporizer. An  
130 improved Ambient (I-A) method was adopted for the elemental ratio analysis of high-resolution  
131 (HR) OA mass spectra, such as oxygen-to-carbon (O:C), and hydrogen-to-carbon (H:C) ratios  
132 (Canagaratna et al., 2015), which reflect the relative composition and oxidation degree for  
133 different OA source. In our study, PMF was performed on HR mass spectra of OA for ions with  
134 *m/z* values of 12-120, together with the signals from integer *m/z* values between 121 to 300 (i.e.,  
135 unit mass resolution, UMR) using SoFi (version 6.3) in Igor Pro (Paatero, 1999; Canonaco et  
136 al., 2013). The data and error matrices were preprocessed according to Elser et al., (2016) and  
137 detailed description of PMF analysis was given elsewhere (Canonaco et al. 2013; Elser et al  
138 2016). Unconstrained PMF solutions with varied factor numbers were analyzed and six factors  
139 were resolved, including two primary and four secondary organic factors (Fig. 3). The six-factor  
140 solution was preferred because the five-factor solution was not able to separate high signal of  
141 *m/z* 44 (which represents high oxidation state) from primary organic aerosol (POA) factors,  
142 while the seven-factor solution added additional OOA factors with similar profiles and noisy  
143 time series for which no physical interpretation could be found. The two POA factors consisted  
144 of a traffic-related factor (hydrocarbon-like OA, HOA) and a cooking-related factor (COA),  
145 which had been resolved in previous summer studies in NCP (Elser et al., 2016; Hu et al., 2016b;  
146 Sun et al., 2016; Huang et al., 2019). AMS source apportionment studies often report one or  
147 two oxygenated organic aerosol (OOA) factors that are distinguished by the extent of  
148 oxygenation and linked to volatility or oxidation degree. Owing to higher mass resolution of  
149 LTOF-AMS and the inclusion of integer-mass signals for *m/z* from 121 to 300 for high-  
150 molecular-weight species such as polycyclic aromatic hydrocarbons (PAHs), we herein  
151 resolved four SOA factors. These four SOA factors include aq-SOA attributable to aqueous-  
152 phase chemistry, ~~phochem-SOA~~ O<sub>x</sub>-initiated-SOA attributable to photochemistry, primary-  
153 related-SOA attributable to prompt oxidation of POA during emission, and fresh-SOA with a  
154 lower *f*<sub>44</sub>/*f*<sub>43</sub> ratio (fraction of *m/z* 44 and 43 in OA).

## 155 2.4 Aerosol liquid water content

156 The aerosol liquid water content (ALWC) was simulated by ISORROPIA-II model  
157 (Fountoukis and Nenes, 2007; Hennigan et al., 2015) using the measurements of ambient  
158 inorganic species (NO<sub>3</sub>, SO<sub>4</sub>, NH<sub>4</sub>, and Chl) and meteorological parameters (temperature and  
159 RH). The simulation was run in “metastable” mode where all components are assumed to be  
160 deliquescent and contain no solid matter. The concentrations and speciation (if dissociated) of  
161 those inorganic species in thermodynamic equilibrium was then simulated by the model and  
162 then the ALWC was calculated. The ISORROPIA-II model does not consider the contribution  
163 to ALWC from organics, since inorganic aerosols dominate the water uptake by ambient  
164 particles with a contribution of approximate >80% of the total ALWC (Huang et al., 2020).

## 165 3. Results and discussion

### 166 3.1 SOA sources

167 In our study, SOA accounted for 69% (13.5  $\mu\text{g m}^{-3}$ ) of the total OA (19.6  $\mu\text{g m}^{-3}$ ),  
168 representing the dominant fraction in OA in summer Handan. Among the four PMF-resolved  
169 SOA sources (Fig. 1), ~~photochem-SOA~~ O<sub>x</sub>-initiated-SOA dominated (31% to total OA), followed  
170 by fresh-SOA (18%), aq-SOA (15%), and primary-related-SOA (5%). Since we focus on SOA  
171 formation in this study, detailed descriptions of the HOA (12%) and COA (19%) is provided in  
172 section 1.1 in the SI. The mass spectral profiles of the six OA source factors are shown in Fig.  
173 1, while the time series of the SOA factors are shown in Fig. 2. In particular, a remarkable  
174 continuous growth of aq-SOA concentration (from  $\sim 0.3 \mu\text{g m}^{-3}$  to  $25.2 \mu\text{g m}^{-3}$ ) and ALWC  
175 (from  $3.1 \mu\text{g m}^{-3}$  to  $486.1 \mu\text{g m}^{-3}$ ) occurred on 24<sup>th</sup>-28<sup>th</sup> August (Fig. 2d). Meanwhile, the O:C  
176 ratio indicative of OA oxidation state displayed a continuous increase from 0.52 to a maximum  
177 of 0.93 during this time (Fig. 2e), consistent with the continuous increase in RH (reaching over  
178 95%). This observation hints that during this period aqueous-phase processing might have  
179 played an important role in aq-SOA formation. This role of aqueous-phase processing in SOA  
180 formation is not just specific to this particular event, but also important in the whole campaign,  
181 which is discussed in detail in section 3.3 later.

182 SOA factors were resolved depending on the oxidation state, which correspond to aged SOA  
183 and fresh SOA respectively (Jimenez et al., 2009). One factor is attributed to aqueous-phase  
184 chemistry (aq-SOA) and the other to photochemistry (~~photochem-SOA~~ O<sub>x</sub>-initiated-SOA), while  
185 fresher factor is produced by fresh-source (fresh-SOA) with a lower  $f_{44}/f_{43}$  ratio, and the other  
186 considered as oxidized primary sources denoted as primary-related-SOA. Although all of the  
187 SOA factors were characterized by higher  $m/z$  44 (CO<sub>2</sub><sup>+</sup>) and  $m/z$  28 (CO<sup>+</sup>) signal compared  
188 with POA factors, their mass spectrum and temporal trends were noticeably distinguishable,

189 corresponding to different formation mechanism, which will be discussed in the following  
190 section.

191 As shown in Fig. S3, the aq-SOA was identified as it increased with ALWC but decreased  
192 with  $O_x$ , which might be produced/influenced by aqueous-phase chemistry and is defined as aq-  
193 SOA. This indicates that aq-SOA was either formed via aqueous phase reactions or  
194 absorbed/dissolved into aerosol liquid water. It exhibits the highest O:C ratios of all factors (0.7)  
195 and a higher  $f_{CO_2+}$  to the total signal of 21.7%, but a low H:C ratio of 1.24 (Fig. 1). The ~~photochem-~~  
196 ~~SOA~~ $O_x$ -initiated-SOA presented an opposite trend with significant increase as function of  $O_x$   
197 but decreased as a function of ALWC (Fig. S3) which is defined as ~~photochem~~ SOA $O_x$ -initiated-  
198 SOA (influenced by photochemistry). As  $O_x$  has been shown to be a conserved tracer to  
199 represent photo-oxidation chemistry (Xu et al., 2017), the relationship between  $O_x$  and  
200 ~~photochem~~ SOA $O_x$ -initiated-SOA can offer insight into the formation mechanism of SOA  
201 associated with the progression of atmospheric photochemical aging (Herndon et al., 2008).

202 The fresh-SOA showed an increase substantially as ALWC increasing, similar to aq-SOA.  
203 Whereas it also showed a slight increase trend following  $O_x$  when  $O_x < 100$  ppb (Fig. S3).  
204 Therefore, both aqueous-phase chemistry and photochemical processing were thought to have  
205 positive impacts synchronously on the formation of fresh-SOA. In this study, the fresh-SOA  
206 had the lowest atomic O:C ratio of 0.41 and the highest atomic H:C ratio of 1.41 among the  
207 four SOA factors, corresponding with the  $f_{CO_2+}$  of 8.3%, these characteristics are consistent with  
208 the global average O:C ratio of LO-OOA of  $0.35 \pm 0.14$ , Ng et al., 2010), demonstrating the it  
209 is more fresh SOA. Although the primary-related-SOA constituted a small fraction and showed  
210 little variation during P1~P3 (3%~5%), this SOA source is also of particular interest because  
211 of its distinctive fragments with high  $m/z$  values in the mass spectrum (Fig. 1d). At  $m/z < 120$ ,  
212 the primary-related-SOA had higher intensities for  $m/z$  43 (mainly  $C_2H_3O^+$ ) and  $m/z$  44 (mainly  
213  $CO_2^+$ ) than those in POA, indicating a typical nature of less-oxidized SOA. At  $m/z > 120$ , PAH-  
214 derived fragments are clearly evident in the mass spectrum of the primary-related-SOA, as  
215 indicated by PAH-like ions (described in SI 1.2) (Dzepina et al., 2007). Previous AMS studies  
216 have observed pronounced peaks of PAH ions in POA mass spectra, such as those in coal  
217 combustion organic aerosol (CCOA) and biomass burning organic aerosol (BBOA) (Hu et al.,  
218 2016b; Zhao et al., 2019), but rarely in SOA. This observation implies that the factor may be  
219 related to the POA originated from domestic coal combustion and here it is termed as primary-  
220 related-SOA (Xu et al., 2006). Moreover, this SOA factor exhibited relatively better  
221 correlations with some gaseous pollutants (Fig. S4), such as CO ( $R = 0.6$ ) and  $NO_2$  ( $R = 0.5$ ),  
222 and also tracked with HOA ( $R = 0.4$ ). These observations suggest that the primary-related-SOA  
223 might be transformed from locally emitted POA as a non-negligible source to SOA.



224 To further investigate the SOA formation mechanism, the dataset was segregated into three  
225 periods according to different features depends on meteorological parameters (Fig. 2), i.e., the  
226 reference period (P1), high-O<sub>x</sub> period (P2) and high-RH period (P3). Briefly, the reference  
227 period, P1, was characterized by a low average OA concentration ( $15.4 \pm 3.2 \mu\text{g m}^{-3}$ ) and was  
228 mainly affected by clean air from southwest of the sampling site and precipitation activities  
229 (Table S1). The high-O<sub>x</sub> period (P2) was featured by a high O<sub>x</sub> concentration ( $65.1 \pm 20.4$  ppb),  
230 warmer temperatures ( $26.4 \pm 4.0$  °C) but lower RH ( $57.7 \pm 17.5$  %). The mass loadings of OA  
231 ( $19.8 \pm 4.7 \mu\text{g m}^{-3}$ ) and other pollutants in P2 were higher than those in P1 (Table S1). P3 was  
232 assigned as a high-RH period because of the noticeably high RH ( $83.7 \pm 12.5$  %) and high  
233 ALWC ( $95.4 \pm 114.2 \mu\text{g m}^{-3}$ ). Winds were weak ( $<1.0 \text{ m s}^{-1}$ ) throughout this period, indicative  
234 of stagnant conditions, which facilitated pollutant accumulation and resulted in the highest  
235 average OA concentrations ( $25.0 \pm 6.2 \mu\text{g m}^{-3}$ ).

236 During the reference period (P1), SOA had the lowest contribution to OA (57%), and the O<sub>x</sub>-  
237 initiated-SOA and aq-SOA constituted 22% and 21% to total OA, respectively. For the high-  
238 O<sub>x</sub> period (P2), enhanced SOA formation was found, with the SOA fraction increased to 71%  
239 of the total OA. The ~~photochem-SOA~~O<sub>x</sub>-initiated-SOA showed the highest mass loading of  $7.3$   
240  $\mu\text{g m}^{-3}$  and highest contribution of 37% to total OA. These increases suggest that high-O<sub>x</sub>  
241 condition facilitates the production of SOA by photochemistry, making the ~~photochem-SOA~~-  
242 initiated-SOA the major source of SOA during P2. During the high-RH period (P3), SOA  
243 fraction continually increased, approaching 79% in total OA, and the SOA was mainly  
244 contributed by aq-SOA and fresh-SOA. The mass contribution of aq-SOA increased  
245 dramatically from 9% to total OA during P2 to 33% during P3 (Fig. S2), and average mass  
246 concentrations from  $1.8 \mu\text{g m}^{-3}$  to  $8.3 \mu\text{g m}^{-3}$ , which suggests rapid SOA production through the  
247 aqueous-phase chemistry. Comparatively, the contribution of fresh-SOA was about ~20% in  
248 both P2 and P3, but lower in P1 (9%), suggesting that the formation fresh-SOA was affected  
249 by both high O<sub>x</sub> and high RH. It should also be noted that O:C ratio increased in the succession  
250 from P1 (0.73) to P2 (0.74) and further to P3 (0.77), accompanied by continually decrease of  
251 H:C ratio from 1.64 to 1.56, and to 1.53 (Fig. 3), suggesting the increase of OA oxidation degree.  
252 As a result, the high O<sub>x</sub> in P2 and high RH in P3 (as compared to P1) promoted the formation  
253 of SOA, specifically ~~photochem-SOA~~O<sub>x</sub>-initiated-SOA (in P2) and aq-SOA (in P3), leading to  
254 the increase in the degree of oxygenation in total OA.

255 ~~Although the primary related SOA constituted a small fraction and showed little variation~~  
256 ~~during P1-P3 (3%~5%), this SOA source is also of particular interest because of its distinctive~~  
257 ~~fragments with high  $m/z$  values in the mass spectrum (Fig. 1d). At  $m/z < 120$ , the primary-~~  
258 ~~related SOA had higher intensities for  $m/z$  43 (mainly  $\text{C}_2\text{H}_3\text{O}^+$ ) and  $m/z$  44 (mainly  $\text{CO}_2^+$ ) than~~  
259 ~~those in POA, indicating a typical nature of less oxidized SOA. At  $m/z > 120$ , PAH derived~~  
260 ~~fragments are clearly evident in the mass spectrum of the primary related SOA, as indicated by~~



261 PAH like ions at  $m/z$  152, 165, 178, 189, 202, 216, 226 + 228, 240 + 242, 250 + 252, 264 +  
262 266, and 276 + 278 (Dzepina et al., 2007). Previous AMS studies have observed pronounced  
263 peaks of PAH ions in POA mass spectra, such as those in coal combustion organic aerosol  
264 (CCOA) and biomass burning organic aerosol (BBOA) (Hu et al., 2016b; Zhao et al., 2019),  
265 but rarely in SOA. This observation implies that the primary related SOA may be related to the  
266 POA originated from domestic coal combustion (Xu et al., 2006). Moreover, this SOA factor  
267 exhibited relatively better correlations with some gaseous pollutants (Fig. S4), such as CO ( $R$   
268 = 0.6) and  $\text{NO}_2$  ( $R = 0.5$ ), and also tracked with HOA ( $R = 0.4$ ). These observations suggest  
269 that the primary related SOA might be transformed from locally emitted POA as a non-  
270 negligible source to SOA. Overall, our results suggest that SOA could be formed through  
271 different pathways, in particular photochemistry, aqueous-phase chemistry, and conversion of  
272 POA to SOA contributed to SOA formation.

### 273 3.2 Photochemistry

274 As expected for summertime, photochemistry associated with  $\text{O}_x$  has significant impacts on  
275 the formation and evolution of SOA. Herein, the relationships between OA factors and  $\text{O}_x$  were  
276 investigated to offer insights into the formation mechanisms of SOA associated with the ozone  
277 production chemistry (Herndon et al., 2008). During P2, as  $\text{O}_x$  increased, the mass loadings of  
278 ~~photochem-SOA~~ $\text{O}_x$ -initiated-SOA showed a substantially increasing trend when  $\text{O}_x$  was > 30 ppb  
279 and eventually saturated when  $\text{O}_x$  was >100 ppb, raising the contribution of ~~photochem-SOA~~ $\text{O}_x$ -  
280 initiated-SOA from 20% to 61% of total OA (Fig. 4). This observation indicates the importance  
281 of photochemistry in the formation of ~~photochem-SOA~~ $\text{O}_x$ -initiated-SOA in summer, in which  
282 high  $\text{O}_x$  concentration as well as temperature corresponding to strong atmospheric oxidative  
283 capacity, can accelerate the photochemical formation (Duan et al., 2021). As a comparison, the  
284 mass concentrations of other OA factors except ~~photochem-SOA~~ $\text{O}_x$ -initiated-SOA showed  
285 decreasing trends as  $\text{O}_x$  increased (Fig. 4c). Such differences between SOA factors are likely  
286 due to the enhanced secondary production/transformation from POA and fresher SOA factors  
287 to the more aged ~~photochem-SOA~~ $\text{O}_x$ -initiated-SOA. Note that the O:C ratio presented a faster  
288 increasing rate as a function of  $\text{O}_x$  (from 0.6 to 1.0, Fig. 4d) than those in P1 and P3, suggesting  
289 that photochemistry might result in higher OA oxidation state during P2.

290 The typical episode with high- $\text{O}_x$  period (P2) was dominated by a series of daytime  
291 photochemical evolutions. To evaluate the relative contributions of photochemical and  
292 aqueous-phase processing production and the transformation of these SOA factors in different  
293 meteorological stages, the average diurnal variations of OA factors, O:C ratios,  $\text{O}_x$ , temperature,  
294 AWLC and primary gas pollutants and RH during different periods are shown for comparison.  
295 Fig. 6 shows that  $\text{O}_x$  increased rapidly from 6:00 to 14:00 in all periods, but was highest in

296 ~~P2. Correspondingly, a lower mean value of ALWC ( $8.4 \mu\text{g m}^{-3}$ ) was also observed in P2 than~~  
297 ~~in P1 and P3. These results are consistent with the increasing trend of T, and similar with~~  
298 ~~ultraviolet radiation in the result in (Li et al., (2020), a driver of photochemical activities,~~  
299 ~~suggesting that the oxidation of OA was enhanced at noon due to photochemical processing.~~  
300 During P2, ~~O<sub>x</sub>-initiated~~-SOA was produced quickly and played the dominant role during  
301 daytime, while its concentration typically decreased during nighttime. The average  
302 concentration of ~~photochem-SOA~~O<sub>x</sub>-initiated-SOA increased continually from  $4.2 \mu\text{g m}^{-3}$  at 7:00  
303 local time (LT) to  $10.4 \mu\text{g m}^{-3}$  at 15:00 LT in 8 h, with the maximum ~~photochem-SOA~~O<sub>x</sub>-  
304 initiated-SOA mass fraction in OA reaching 65% at 15:00 LT (Fig. S6c). This high average  
305 growth rate of  $0.8 \mu\text{g m}^{-3} \text{ h}^{-1}$  in ~~photochem~~-O<sub>x</sub>-initiated-SOA corresponded to the high O<sub>x</sub>  
306 concentration, high temperature and strong solar radiation in daytime, suggesting enhanced  
307 photochemistry reaction. In contrast, the concentrations and the contributions of other SOA  
308 factors decreased continuously at the same time (Fig. 6). ~~The opposite trends between O<sub>x</sub>-~~  
309 ~~initiated-SOA and other OA factors from 7:00 to 15:00 LT suggest that some part of POA and~~  
310 ~~fresh-SOA may convert to O<sub>x</sub>-initiated-SOA by photochemical oxidation. This conclusion is~~  
311 ~~consistent with findings reported by Li et al., (2020) in urban Beijing, where less-oxidized SOA~~  
312 ~~may transform to more-oxidized SOA through photochemical processing as well. The O:C ratio~~  
313 ~~of OA presented a significant increasingly diurnal variation with a noon peak around 14:00 ~~~  
314 ~~16:00 LT in P2, which had the highest value of 0.74 compared with it in P1 and P3, suggesting~~  
315 the potential transformation from POA factors and fresh SOA factors to ~~photochem-SOA~~ O<sub>x</sub>-  
316 initiated-SOA could also noticeably affect OA characteristics such as oxidation state in summer  
317 daytime. ~~The O:C ratio of OA also presented a significant increasingly diurnal variation with a~~  
318 ~~noon peak around 14:00 ~ 16:00 in P2, which had the highest value of 0.74 compared with it~~  
319 ~~in P1 and P3. It is further indicated by a small afternoon peak of the more oxidized tracer CO<sub>2</sub><sup>±</sup>~~  
320 ~~(*m/z* 44) and the decrease in a less oxidized tracer C<sub>2</sub>H<sub>3</sub>O<sup>+</sup> (*m/z* 43) (Fig. 7b). As a result, the~~  
321 ~~mass spectra, which were initially fresh SOA products evolved to become aged SOA products~~  
322 ~~as the photochemical age increased. Overall, with little water in the particles, the high solar~~  
323 ~~radiation and high O<sub>x</sub> concentration during daytime associated with a relatively high degree of~~  
324 ~~oxygenation of OA suggest that gas-phase oxidation and partitioning processes are probably~~  
325 ~~the dominating process in SOA formation during P2.~~

326 In addition, these results further support the idea that during the high-O<sub>x</sub> period of summer,  
327 photochemistry has significant impacts on SOA formation, especially on ~~photochem~~-O<sub>x</sub>-initiated-  
328 SOA. Note that the role of photochemistry in the formation of ~~photochem~~-O<sub>x</sub>-initiated-SOA is  
329 not only limited to the gas-phase photochemistry, but also can also occur in the aqueous phase  
330 (Kuang et al., 2020). This is the case for P3 in our study, which is discussed further in section  
331 3.3 below.

332

### 333 3.3 Aqueous-phase chemistry

334 The aqueous-phase chemistry has imposed significant impacts on SOA formation during  
335 this field campaign. To further explore the formation mechanism of SOA associated with  
336 aqueous-phase chemistry, the relationships between different OA factors and ALWC were  
337 investigated. During P3, the mass concentration of aq-SOA increased from  $5 \mu\text{g m}^{-3}$  to  $17 \mu\text{g}$   
338  $\text{m}^{-3}$ , yet its fraction showed a particularly pronounced rise from 22.5% to 52% of total OA when  
339 ALWC increased from 0.3 to  $200 \mu\text{g m}^{-3}$  (Fig. 5e and f). Note that the strong correlation between  
340 aq-SOA and ALWC was not only observed in P3. Rather, the time series of aq-SOA and ALWC  
341 were remarkably well correlated throughout the entire campaign ( $R=0.7$ , Fig. S4). This general  
342 correlation further confirms the important role of aqueous-phase chemistry in the formation of  
343 aq-SOA and characterized the aqueous-phase formation of aq-SOA throughout the campaign  
344 rather than only in the high-RH event as shown in section 3.1 earlier. We also found that the  
345 concentration and fraction of aq-SOA became stable when ALWC was  $> 200 \mu\text{g m}^{-3}$ , which is  
346 probably attributable to that the aq-SOA formation within droplets was soon outweighed by the  
347 scavenging processes when RH was high enough ( $> 95\%$ ). ~~Fig. 5e shows that the fresh SOA~~  
348 ~~has similar increasing trend with aq-SOA as ALWC increased, which suggests that aqueous-~~  
349 ~~phase chemistry might have also played an important role in the formation of fresh SOA. The~~  
350 ~~fresh SOA also increased slightly as  $\text{O}_x$  increased (Fig. 4e), suggesting that both the aqueous-~~  
351 ~~phase chemistry and the photochemistry (including that in the aqueous phase) participated to~~  
352 ~~produce fresh SOA simultaneously. The O:C ratio shows an obvious increase from 0.7 to~~  
353 ~~around 0.85 when ALWC increases to  $200 \mu\text{g m}^{-3}$ , after which it remains relatively stable (0.85)~~  
354 ~~as the ALWC increases further (Fig. 5). These results suggest that aqueous-phase chemistry can~~  
355 ~~affect the oxidation degree of OA by changing SOA composition, especially the enhanced~~  
356 ~~contribution of aq-SOA. However, the growth rate of O:C ratios as ALWC increases in P3 was~~  
357 ~~lower than that in P2 (up to 1 as  $\text{O}_x$  increases). Also, the correlation between O:C vs.  $\text{O}_x$  in P2~~  
358 ~~( $R=0.6$ ) was stronger than O:C vs. ALWC ( $R=0.3$ ) (Fig. S8). This result illustrates that~~  
359 ~~photochemistry is more efficient in elevating the oxidation degree of OA than is the aqueous-~~  
360 ~~phase chemistry.~~

361 Fig. 6 illustrate the different types of aqueous-phase chemistry in daytime and nighttime.  
362 During the nighttime in P3, aqueous-phase oxidation was also enhanced during nighttime  
363 (19:00–07:00 LT). As shown in Fig. 6, O:C ratio (0.76) at nighttime in P3 was higher than those  
364 in P2, while exhibiting a much smaller peak during daytime. Compared with the low ALWC in  
365 P2, the much higher ALWC concentration (peak value of  $235.9 \mu\text{g m}^{-3}$  at 2:00 LT) and higher  
366 RH (peak value of 93.7% at 6:00 LT) during nighttime in P3 suggested a dominant contribution  
367 by aqueous-phase processing. The aq-SOA shows a quite clear and unique diurnal pattern in  
368 P3, with much higher mass concentration during the whole day (especially at nighttime) than

369 those in P1 and P2. After 17:00 LT, aq-SOA started to increase from  $4.7 \mu\text{g m}^{-3}$  to  $12.7 \mu\text{g m}^{-3}$   
370 at 7:00 LT, which showed a rapid nighttime growth rate of  $0.6 \mu\text{g m}^{-3} \text{h}^{-1}$ , indicating enhanced  
371 SOA formation through aqueous-phase chemistry at night. Whereas  $\text{O}_x$ -initiated-SOA  
372 decreased rapidly from  $8.2 \mu\text{g m}^{-3}$  at 17:00 LT until reaching its lowest concentration of  $2.6$   
373  $\mu\text{g m}^{-3}$  until the morning, suggesting the gas-to-particle partitioning at night under high ALWC  
374 conditions. Furthermore, this transformation could be supported by the increase in  $\text{CO}_2^+$  ( $m/z$   
375 44) and the decrease in a less oxidized tracer  $\text{C}_2\text{H}_3\text{O}^+$  ( $m/z$  43) at night (Fig. 7c). Since –when  
376 the ALWC is sufficiently high, it was likely to accommodate much of the precursor organics  
377 and oxidants to low-volatility products through aqueous-phase oxidation. In addition, the dark  
378 aqueous-phase SOA formation was likely strong enough to counteract the nighttime scavenging  
379 processes under high-RH conditions. Therefore, the dark aqueous-phase chemistry forming aq-  
380 SOA shows a dominant role (over 40% to OA) during nighttime in P3.

381 ~~However, The aq SOA shows a quite clear and unique diurnal pattern in P3, with much~~  
382 ~~higher mass concentration during the whole day (especially at nighttime) than those in P1 and~~  
383 ~~P2. This may be attributed to the stagnant meteorological conditions and high RH (thus ALWC),~~  
384 ~~which facilitated the continuous formation of aq SOA in P3.~~ during the daytime, the mass  
385 concentration of aq-SOA decreased from 7:00 to 17:00 LT in P3, coinciding an obvious  
386 increase trend of  $\text{O}_x$ -initiated-SOA at the same time with an average growth rate of  $0.6 \mu\text{g m}^{-3}$   
387  $\text{h}^{-1}$  (Fig. 6). This phenomenon suggests photochemical processing can also occur in the aqueous  
388 phase when RH and ALWC were still high, consistent with the decrease of RH and the increase  
389 of temperature (Fig. 6S7). ~~W~~In addition, we also noticed that significant photochem SOA  
390 initiated-SOA formation also occurred during daytime in P3 with an average growth rate of  
391  $0.6 \mu\text{g m}^{-3} \text{h}^{-1}$ . This observation is similar to results in a previous study showing that both  
392 aqueous phase and gas phase photochemical reactions substantially contributed to the  
393 formation of OOA (a surrogate of SOA) during the high RH period (Kuang et al., 2020). The  
394 rapid daytime photochem SOA formation in our study probably occurred in the aqueous phase  
395 driven by photochemical reactions during daytime under humid conditions with high ALWC.  
396 ~~The  $\text{O}_x$  initiated SOA increased from  $2.6 \mu\text{g m}^{-3}$  at 7:00 LT until reaching its highest~~  
397 ~~concentration of  $8.2 \mu\text{g m}^{-3}$  at 16:00 LT with an average growth rate of  $0.6 \mu\text{g m}^{-3} \text{h}^{-1}$  and then~~  
398 ~~decreased rapidly until night, coinciding with obvious decrease trend of aq SOA at the same~~  
399 ~~time. This distinct trends further suggest that the transformation of gas particle partitioning~~  
400 ~~through aqueous phase chemistry at daytime.~~ Photochemical reactions through both aqueous-  
401 phase and gas-phase can contribute substantially to the SOA formation in polluted areas of NCP,  
402 and during haze days with high RH and ALWC the aqueous-phase photochemical processes  
403 played a dominant role in daytime SOA formation (Kuang et al., 2020). The rapid daytime  $\text{O}_x$ -  
404 initiated-SOA formation in our study possibly occurred on the particle surface and in the aerosol  
405 liquid water (Ervens et al., 2011) under humid conditions with high ALWC but driven by gas-

406 phase direct photolysis and oxidation by photooxidants under high  $O_x$  conditions. Under such  
407 high-RH level ( $RH > 80\%$ ), the water-soluble species produced from photochemistry in the gas  
408 phase can also partition into the aqueous phase and be further oxidized to form low-volatility  
409 products (Carlton et al., 2007; Sullivan et al., 2016). Previous studies have demonstrated that  
410 gas-phase oxidants such as OH radicals and  $H_2O_2$  can also partition to the aqueous phase to  
411 further oxidize dissolved the oxidized VOCs (OVOCs) into aq-SOA (Ye et al., 2018). Other  
412 studies also revealed that photochemical reactions in the aqueous droplets can occur through  
413 direct photolysis or through oxidation by oxidants (Ervens et al., 2011; 2014; Ye et al., 2018).  
414 Therefore, in our campaign, dark aqueous-phase chemistry is responsible for rapid aq-SOA  
415 formation during nighttime, while the aqueous-phase photochemistry during daytime is likely  
416 prevail by rapid daytime ~~photochem~~  $O_x$ -initiated-SOA formation during P3. This comparison  
417 demonstrates that the nocturnal aqueous-phase chemistry and daytime aqueous-phase  
418 photochemistry are both important pathways in the total SOA growth.

419 The aqueous-phase chemistry related to fresh-SOA is more complicated, requiring both  
420 daytime radiative conditions and certain amounts of ALWC in nighttime. For example, Fig. 5e  
421 shows that the fresh-SOA has a similar increasing trend with aq-SOA as ALWC increased,  
422 however, it also increased slightly as  $O_x$  increased (Fig. 4e), hinting that both ALWC and the  
423 oxidants are critical for fresh-SOA formation and both the aqueous-phase chemistry and the  
424 photochemistry (including that in the aqueous phase) participated to produce fresh-SOA  
425 simultaneously. It is worth noting that three peaks were found in the diurnal variation of fresh-  
426 SOA in P3. The peaks at around 6:00 and 19:00 LT at night were similar to those of aq-SOA  
427 and lower than it, while the peak at around 13:00 LT is consistent with the peak in the diurnal  
428 cycle of  $O_x$  (Fig. 6). Although there is also a smaller peak around 13:00 LT in P3, the whole  
429 pattern of aq-SOA is characterized by decreasing trend at daytime. These results suggest that  
430 fresh-SOA could be formed through dark nighttime aqueous-phase reactions, which are  
431 partially reversible upon the evaporation of aerosol liquid water, and also formed through  
432 photochemical aqueous-phase reactions during daytime. Different from aq-SOA, which is  
433 highly correlated and limited with ALWC, two types of aqueous-phase chemistry in daytime  
434 and nighttime are dominant pathways to the fresh-SOA growth. This three-peak diurnal pattern  
435 hints that both the dark aqueous-phase chemistry and the daytime photochemistry (either in the  
436 gas phase or in the aqueous phase) are important in the formation of fresh SOA.—Our analysis  
437 on formation pathways of these SOA factors suggested the potential interactive roles of gas-  
438 phase oxidation, gas-particle partitioning, and aqueous-phase oxidation in the formation of  
439 SOA.

#### 440 **3.4 SOA from POA transformation**



441 The photochemistry and aqueous-phase chemistry show distinct effects on POA evolution  
442 and SOA formation. The relationships between ~~phochem-SOA~~O<sub>x</sub>-initiated-SOA /aq-SOA and  
443 other POA-related components (HOA + COA + primary-related-SOA) were plotted in Fig. S9.  
444 A strong negative correlation ( $R=-0.8$ ) between POA-related components and ~~phochem-SOA~~  
445 O<sub>x</sub>-initiated-SOA was observed (Fig. S9c), consistent with the decrease in mass concentration  
446 of POA-related components during P2. This observation suggests that the production of  
447 ~~phochem-SOA~~O<sub>x</sub>-initiated-SOA was at least partly facilitated by photochemical transformation  
448 of other OA components. However, the better diffusion conditions in P2 might also attribute a  
449 great extent to the negative correlation, as the formation period of O<sub>x</sub>-initiated-SOA usually  
450 occurred during the noontime when the boundary layer was much developed, while the POA  
451 usually decreased via horizontal and vertical diffusion. In addition, compared with P1 and P3,  
452 a more positive promotion on the phochem-SOA O<sub>x</sub> initiated SOA formation was observed in  
453 P2 when O<sub>x</sub> was more than 40 ppb. These observations confirm the results in section 3.2 that  
454 intensive formation of phochem-SOA O<sub>x</sub> initiated SOA was not only produced by  
455 photochemical oxidation from VOCs at high O<sub>x</sub> levels, but also potentially through the  
456 transformation of POA related components into phochem-SOA O<sub>x</sub> initiated SOA. In  
457 comparison, POA-related components and aq-SOA correlate weakly. When ALWC ( $<20 \mu\text{g}$   
458  $\text{m}^{-3}$ ) and nitrate concentrations were lower ( $< 3 \mu\text{g} \text{m}^{-3}$ ), mostly during P1 and P2, POA-related  
459 components and aq-SOA showed almost no correlation ( $R=0.1$  and  $R=-0.1$ ). However, when  
460 ALWC concentration and nitrate concentration were higher than those thresholds above (data  
461 points with yellow/red colors mostly during P3), they had a relatively good negative correlation  
462 ( $R=-0.5$ ) (Fig. S9f), indicating the importance of ALWC and nitrate in aqueous-phase chemistry.  
463 This is consistent with results in winter Beijing (Wang et al., 2021), where POA factor had  
464 strong negative correlations with aq-SOA, suggesting that these POA factors might produce aq-  
465 SOA by aqueous-phase oxidation. In addition, under high-ALWC conditions, nitrate had  
466 similar formation mechanisms with aq-SOA or high nitrate supports the potential  
467 formation/transformation from POA-related components to aq-SOA, which is consistent with  
468 the results in section 3.3. The phenomenon of negative correlation between POA-related  
469 components and SOA at high O<sub>x</sub>/ALWC further emphasizes the importance of conversion from  
470 POA to SOA.

471 As shown in the Van Krevelen (VK) plot (Fig. 8a), O:C and H:C both increase in the  
472 succession from primary-related-SOA to ~~phochem-SOA~~O<sub>x</sub>-initiated-SOA and eventually to aq-  
473 SOA, supporting a successive oxidation sequence from primary-related-SOA to aq-SOA.  
474 Generally, H:C shows a decreasing trend as O:C increases for organic compounds during  
475 oxidation in other studies (Ng et al., 2011; Gilardoni et al., 2016; Lee et al., 2017; Zhao et al.,  
476 2019; Chen et al., 2021), suggesting a general negative correlation between H:C and O:C. This  
477 positive relationship of O:C and H:C evolution during oxidative aging in this study is interesting.

478 It might be caused by ring-breaking reactions which could further promote the transformation  
479 of aromatic POA to aq-SOA. Previous studies in both laboratory (Huang et al., 2018; Wang et  
480 al., 2020) and field (Hu et al., 2016a) demonstrated that the OH-initiated ring-breaking reactions  
481 of aromatic species can occur in the aqueous phase and form highly oxidized oxygenated  
482 compounds. For example, Hems and Abbatt (2018) suggested that nitrophenol molecules could  
483 react rapidly with OH radicals in aqueous solutions with the addition of OH functional groups  
484 to the aromatic ring at the initial stage, followed by fragmentation to multifunctional organic  
485 species with high H:C and O:C ratios. Wang et al. (2021) found that the ring-breaking oxidation  
486 of aromatic FF-POA was the mechanism for aq-SOA formation. Similar to those in primary-  
487 related-SOA, PAH-like ions was also found in the mass spectrum of aq-SOA at  $m/z > 150$ ,  
488 albeit less pronounced, consistent with a previous study in Beijing (Wang et al., 2021). This is  
489 likely due to the oxidation of PAHs in the conversion of primary-related-SOA and aq-SOA,  
490 which is caused by enhanced hydroxylation of the aromatic ring and increased yields of  
491 carboxylic acids in OH-initiated reactions (Sun et al., 2010). This kind of ring-breaking  
492 oxidation of aromatic POA could thus lead to aq-SOA formation (Huang et al., 2018; Wang et  
493 al., 2021). In addition, the locations of aq-SOA and the slope of overall OA are near the line  
494 with the slope of -1 in the VK plot, indicating more carboxylic acid formation while the  
495 replacement of a hydrogen atom with a carboxylic acid group ( $-\text{COOH}$ ) (Heald et al., 2010;  
496 Ng et al., 2011). This observation supports that oxidation of PAHs was probably involved in  
497 the conversion of primary-related-SOA to aq-SOA through aqueous-phase chemistry, leading  
498 to functionalization as carbonyls and carboxylic acids.

499 Specifically, the organic fragments and mass spectrum evolution of OA were analyzed to  
500 illuminate the transformation in photochemical processing and aqueous-phase chemistry. Fig.  
501 8b shows the mass fractions of  $\text{CH}_2\text{O}_2^+$ ,  $\text{CH}_3\text{SO}^+$ ,  $\text{HCO}_2^+$ , and  $\text{C}_2\text{H}_2\text{O}_2^+$  ion fragments in OA as  
502 a function of ALWC. The aq-SOA was tightly correlated with  $\text{CH}_2\text{O}_2^+$  ( $R^2 = 0.81$ ) at  $m/z$  46  
503 and  $\text{CH}_3\text{SO}$  ( $R^2 = 0.78$ ) at  $m/z$  63 (Fig. S10). Consistently, both of them showed increase trends  
504 as ALWC increasing, similar as aq-SOA, which indicating typical fragment characteristics of  
505 ions of aqueous-phase processing products (Tan et al., 2009; Sun et al., 2016; Duan et al., 2021).  
506 The intensities of  $\text{HCO}_2^+$  ( $m/z$  45), a common fragment ion of carboxylic acids, is associated  
507 with aqueous oxidation of aromatic compounds.  $\text{C}_2\text{H}_2\text{O}_2^+$  ( $m/z$  58) is a tracer ion for glyoxal,  
508 which could be a ring-breaking product from the aqueous-phase oxidation of PAHs. The  
509 increasing trends of these ions with ALWC suggest that water-soluble organic species such as  
510 carboxylic acids and glyoxal are produced as components of aq-SOA following aromatic  
511 oxidation and ring breaking. Moreover, the concentration of PAHs increased with the increase  
512 of ALWC (Fig. S11), consistent with the oxidation of PAHs from ring-breaking reactions that  
513 can take place in the aqueous phase and being involved in the conversion to aq-SOA.



#### 514 4. Conclusion

515 The sources and formation mechanisms of SOA were investigated by online aerosol mass  
516 spectrometry and statistical (PMF) analysis from August to September of 2019 in Handan, a  
517 mid-sized industrialized city in NCP of China. Four specific SOA factors were resolved,  
518 including aq-SOA (15% to total OA), ~~photochem-SOA~~<sub>O<sub>x</sub></sub>-initiated-SOA (31%), fresh-SOA (18%)  
519 and primary-related-SOA (5%). By studying the formation of these SOA factors in different  
520 selected periods (P1-P3) against O<sub>x</sub> and ALWC, we found multiple pathways leading to their  
521 formation, sometimes with mixed pathways for one type of SOA.

522 Both photochemistry and aqueous-phase chemistry resulted in enhanced OA oxidation state;  
523 ~~but the effect of photochemistry was stronger in SOA formation.~~ During high-O<sub>x</sub> period,  
524 photochemistry had imposed significant impacts on the formation and evolution of SOA in  
525 summertime. The ~~photochem-SOA~~<sub>O<sub>x</sub></sub>-initiated-SOA contributed up to 65% to total OA in the  
526 daytime, with a high average growth rate of 0.8 μg m<sup>-3</sup> h<sup>-1</sup>, suggesting the efficient daytime  
527 formation of SOA from photochemistry. Rapid increases of the concentration and contribution  
528 (up to 61%) of ~~photochem-SOA~~<sub>O<sub>x</sub></sub>-initiated-SOA were found as O<sub>x</sub> increased, while all the other  
529 OA factors showed decreasing trends with O<sub>x</sub> concentration increasing. The difference suggests  
530 enhanced secondary transformation from POA/fresh SOA factors to the more aged ~~photochem-~~  
531 ~~SOA~~<sub>O<sub>x</sub></sub>-initiated-SOA under high-O<sub>x</sub> condition. However, during the high-RH period, two  
532 types of aqueous-phase chemistry were both important pathways for the SOA growth. During  
533 nighttime and under high-RH conditions, dark aqueous-phase chemistry played significant  
534 roles with rapid aq-SOA formation (up to 45% in total OA), while the aqueous-phase  
535 photochemistry was more important by rapid ~~photochem-SOA~~<sub>O<sub>x</sub></sub>-initiated-SOA formation  
536 during daytime (up to 39% in total OA). The primary-related-SOA was evidently linked to the  
537 POA originated from coal combustion activities, as indicated by the PAH-like ion peaks.  
538 Although it constituted a small fraction of 5%, the potential transformation and conversion from  
539 primary-related-SOA to aq-SOA could also be an important pathway via hydroxylation of the  
540 aromatic ring or ring-breaking oxidation of aromatic POA species through aqueous-phase  
541 chemistry. This study highlights the multiple reaction pathways, on top of multiple precursor  
542 types, on the SOA formation in industrialized regions, and calls form more in-depth study on  
543 the interactive roles of those formation pathways.

544

545 **Data availability.** Raw data used in this study are archived at the Institute of Earth Environment,  
546 Chinese Academy of Sciences, and are available on request by contacting the corresponding  
547 author.

548 **Supplement.** The Supplement related to this article is available online.

549 **Competing interests.** The authors declare that they have no conflict of interest.

550 **Author contributions.** RJH designed the study. Data analysis and source apportionment were  
551 done by YFG and RJH. YFG and RJH wrote the manuscript. YFG and RJH interpreted data  
552 and prepared display items. All authors commented on and discussed the manuscript.

### 553 **Acknowledgement**

554 This work was supported by the National Natural Science Foundation of China (no.  
555 41925015), the Key Research Program of Frontier Sciences from the Chinese Academy of  
556 Sciences (no. ZDBS-LY-DQC001), the Strategic Priority Research Program of the Chinese  
557 Academy of Sciences (no. XDB40000000), and SKLLQG (no. SKLLQGTD1801).

558

559 **References**

560 An, Z., Huang, R. J., Zhang, R., Tie, X., Li, G., Cao, J., Zhou, W., Shi, Z., Han, Y., Gu, Z., and  
561 Ji, Y.: Severe haze in northern China: A synergy of anthropogenic emissions and  
562 atmospheric processes, *Proc. Natl. Acad. Sci. U. S. A.*, 116, 8657–8666,  
563 <https://doi.org/10.1073/pnas.1900125116>, 2019.

564 Bikkina, S., Kawamura, K., and Sarin, M.: Secondary Organic Aerosol Formation over Coastal  
565 Ocean: Inferences from Atmospheric Water-Soluble Low Molecular Weight Organic  
566 Compounds, *Environ. Sci. Technol.*, 51, 4347–4357,  
567 <https://doi.org/10.1021/acs.est.6b05986>, 2017.

568 Canagaratna, M. R., Jimenez, J. L., Kroll, J. H., Chen, Q., Kessler, S. H., Massoli, P.,  
569 Hildebrandt Ruiz, L., Fortner, E., Williams, L. R., Wilson, K. R., Surratt, J. D., Donahue, N.  
570 M., Jayne, J. T., and Worsnop, D. R.: Elemental ratio measurements of organic compounds  
571 using aerosol mass spectrometry: Characterization, improved calibration, and implications,  
572 *Atmos. Chem. Phys.*, 15, 253–272, <https://doi.org/10.5194/acp-15-253-2015>, 2015.

573 Canonaco, F., Crippa, M., Slowik, J. G., Baltensperger, U., and Prévôt, A. S. H.: SoFi, an  
574 IGOR-based interface for the efficient use of the generalized multilinear engine (ME-2) for  
575 the source apportionment: ME-2 application to aerosol mass spectrometer data, *Atmos.*  
576 *Meas. Tech.*, 6, 3649–3661, <https://doi.org/10.5194/amt-6-3649-2013>, 2013.

577 Carlton, A. G., Turpin, B. J., Altieri, K. E., Seitzinger, S., Reff, A., Lim, H. J., and Ervens, B.:  
578 Atmospheric oxalic acid and SOA production from glyoxal: Results of aqueous  
579 photooxidation experiments, *Atmos. Environ.*, 41, 7588–7602,  
580 <https://doi.org/10.1016/j.atmosenv.2007.05.035>, 2007.

581 Chen, W., Ye, Y., Hu, W., Zhou, H., Pan, T., Wang, Y., Song, W., Song, Q., Ye, C., Wang, C.,  
582 Wang, B., Huang, S., Yuan, B., Zhu, M., Lian, X., Zhang, G., Bi, X., Jiang, F., Liu, J.,  
583 Canonaco, F., Prevot, A. S. H., Shao, M., and Wang, X.: Real-time characterization of  
584 aerosol compositions, sources and aging processes in Guangzhou during PRIDE-GBA 2018  
585 campaign, *J. Geophys. Res. Atmos.*, <https://doi.org/10.1029/2021jd035114>, 2021.

586 Cohen, A. J., Brauer, M., Burnett, R., Anderson, H. R., Frostad, J., Estep, K., Balakrishnan, K.,  
587 Brunekreef, B., Dandona, L., Dandona, R., Feigin, V., Freedman, G., Hubbell, B., Jobling,  
588 A., Kan, H., Knibbs, L., Liu, Y., Martin, R., Morawska, L., Pope, C. A., Shin, H., Straif, K.,  
589 Shaddick, G., Thomas, M., van Dingenen, R., van Donkelaar, A., Vos, T., Murray, C. J. L.,  
590 and Forouzanfar, M. H.: Estimates and 25-year trends of the global burden of disease  
591 attributable to ambient air pollution: an analysis of data from the Global Burden of Diseases  
592 Study 2015, *Lancet*, 389, [https://doi.org/10.1016/S0140-6736\(17\)30505-6](https://doi.org/10.1016/S0140-6736(17)30505-6), 2017.

593 Donahue, N. M., Robinson, A. L., Stanier, C. O., and Pandis, S. N.: Coupled partitioning,  
594 dilution, and chemical aging of semivolatile organics, *Environ. Sci. Technol.*, 40,  
595 <https://doi.org/10.1021/es052297c>, 2006.

- 596 Duan, J., Huang, R. J., Gu, Y., Lin, C., Zhong, H., Wang, Y., Yuan, W., Ni, H., Yang, L., Chen,  
597 Y., Worsnop, D. R., and O'Dowd, C.: The formation and evolution of secondary organic  
598 aerosol during summer in Xi'an: Aqueous phase processing in fog-rain days, *Sci. Total*  
599 *Environ.*, 756, 144077, <https://doi.org/10.1016/j.scitotenv.2020.144077>, 2021.
- 600 Dzepina, K., Arey, J., Marr, L. C., Worsnop, D. R., Salcedo, D., Zhang, Q., Onasch, T. B.,  
601 Molina, L. T., Molina, M. J., and Jimenez, J. L.: Detection of particle-phase polycyclic  
602 aromatic hydrocarbons in Mexico City using an aerosol mass spectrometer, *Int. J. Mass*  
603 *Spectrom.*, 263, 152–170, <https://doi.org/10.1016/j.ijms.2007.01.010>, 2007.
- 604 Elser, M., Huang, R., Wolf, R., Slowik, J. G., Wang, Q., Canonaco, F., Li, G., Bozzetti, C.,  
605 Daellenbach, K. R., Huang, Y., Zhang, R., Li, Z., Cao, J., Baltensperger, U., El-haddad, I.,  
606 and Prévôt, A. S. H.: New insights into PM<sub>2.5</sub> chemical composition and sources in two  
607 major cities in China during extreme haze events using aerosol mass spectrometry, 3207–  
608 3225, <https://doi.org/10.5194/acp-16-3207-2016>, 2016.
- 609 Ervens, B., Turpin, B. J., and Weber, R. J.: Secondary organic aerosol formation in cloud  
610 droplets and aqueous particles (aqSOA): A review of laboratory, field and model studies,  
611 *Atmos. Chem. Phys.*, 11, 11069–11102, <https://doi.org/10.5194/acp-11-11069-2011>, 2011.
- 612 Ervens, B., Armin, S., B., L. Y., and J., and T. B.: Key parameters controlling OH-initiated  
613 formation of secondary organic aerosol in the aqueous phase (aqSOA), *J. Geophys. Res.*,  
614 6578–6595, <https://doi.org/10.1002/2013JD021021>.Received, 2014.
- 615 Fountoukis, C. and Nenes, A.: ISORROPIAII: A computationally efficient thermodynamic  
616 equilibrium model for K<sup>+</sup>-Ca<sup>2+</sup>-Mg<sup>2+</sup>-NH<sub>4</sub><sup>+</sup>-Na<sup>+</sup>-SO<sub>4</sub><sup>2-</sup>-NO<sub>3</sub><sup>-</sup>-Cl<sup>-</sup>-H<sub>2</sub>O aerosols, *Atmos.*  
617 *Chem. Phys.*, 7, 4639–4659, <https://doi.org/10.5194/acp-7-4639-2007>, 2007.
- 618 Gilardoni, S., Massoli, P., Paglione, M., Giulianelli, L., Carbone, C., Rinaldi, M., Decesari, S.,  
619 Sandrini, S., Costabile, F., and Gobbi, G. P.: Direct observation of aqueous secondary  
620 organic aerosol from biomass-burning emissions, *Proc. Natl. Acad. Sci. U. S. A.*, 113,  
621 10013–10018, <https://doi.org/10.1073/pnas.1602212113>, 2016.
- 622 Gu, Y., Huang, R. J., Li, Y., Duan, J., Chen, Q., Hu, W., Zheng, Y., Lin, C., Ni, H., Dai, W.,  
623 Cao, J., Liu, Q., Chen, Y., Chen, C., Ovadnevaite, J., Ceburnis, D., and O'Dowd, C.:  
624 Chemical nature and sources of fine particles in urban Beijing: Seasonality and formation  
625 mechanisms, *Environ. Int.*, 140, 105732, <https://doi.org/10.1016/j.envint.2020.105732>,  
626 2020.
- 627 Heald, C. L., Kroll, J. H., Jimenez, J. L., Docherty, K. S., Decarlo, P. F., Aiken, A. C., Chen,  
628 Q., Martin, S. T., Farmer, D. K., and Artaxo, P.: A simplified description of the evolution  
629 of organic aerosol composition in the atmosphere, *Geophys. Res. Lett.*, 37,  
630 <https://doi.org/10.1029/2010GL042737>, 2010.
- 631 Hems, R. F. and Abbatt, J. P. D.: Aqueous Phase Photo-oxidation of Brown Carbon  
632 Nitrophenols: Reaction Kinetics, Mechanism, and Evolution of Light Absorption, *ACS*  
633 *Earth Sp. Chem.*, 2, 225–234, <https://doi.org/10.1021/acsearthspacechem.7b00123>, 2018.

- 634 Hennigan, C. J., Izumi, J., Sullivan, A. P., Weber, R. J., and Nenes, A.: A critical evaluation of  
635 proxy methods used to estimate the acidity of atmospheric particles, *Atmos. Chem. Phys.*,  
636 15, 2775–2790, <https://doi.org/10.5194/acp-15-2775-2015>, 2015.
- 637 Herndon, S. C., Onasch, T. B., Wood, E. C., Kroll, J. H., Canagaratna, M. R., Jayne, J. T.,  
638 Zavala, M. A., Knighton, W. B., Mazzoleni, C., Dubey, M. K., Ulbrich, I. M., Jimenez, J.  
639 L., Seila, R., de Gouw, J. A., de Foy, B., Fast, J., Molina, L. T., Kolb, C. E., and Worsnop,  
640 D. R.: Correlation of secondary organic aerosol with odd oxygen in Mexico City, *Geophys.*  
641 *Res. Lett.*, 35, <https://doi.org/10.1029/2008GL034058>, 2008.
- 642 Hu, W., Hu, M., Hu, W. W., Niu, H., Zheng, J., Wu, Y., Chen, W., Chen, C., Li, L., Shao, M.,  
643 Xie, S., and Zhang, Y.: Characterization of submicron aerosols influenced by biomass  
644 burning at a site in the Sichuan Basin, southwestern China, *Atmos. Chem. Phys.*, 16, 13213–  
645 13230, <https://doi.org/10.5194/acp-16-13213-2016>, 2016a.
- 646 Hu, W., Hu, M., Hu, W., Jimenez, J. L., Yuan, B., Chen, W., Wang, M., Wu, Y., Chen, C.,  
647 Wang, Z., Peng, J., Zeng, L., and Shao, M.: *Journal of Geophysical Research : Atmospheres*,  
648 1955–1977, <https://doi.org/10.1002/2015JD024020>.Received, 2016b.
- 649 Hu, W., Palm, B. B., Day, D. A., Campuzano-Jost, P., Krechmer, J. E., Peng, Z., De Sa Suzane,  
650 S., Martin, S. T., Alexander, M. L., Baumann, K., Hacker, L., Kiendler-Scharr, A., Koss, A.  
651 R., De Gouw, J. A., Goldstein, A. H., Seco, R., Sjostedt, S. J., Park, J. H., Guenther, A. B.,  
652 Kim, S., Canonaco, F., Prévôt, A. S. H., Brune, W. H., and Jimenez, J. L.: Volatility and  
653 lifetime against OH heterogeneous reaction of ambient isoprene-epoxydiols-derived  
654 secondary organic aerosol (IEPOX-SOA), *Atmos. Chem. Phys.*, 16, 11563–11580,  
655 <https://doi.org/10.5194/acp-16-11563-2016>, 2016c.
- 656 Hu, W., Hu, M., Hu, W., Zheng, J., Chen, C., Wu, Y., and Guo, S.: Seasonal variations in high  
657 time-resolved chemical compositions, sources, and evolution of atmospheric submicron  
658 aerosols in the megacity Beijing, 9979–10000, 2017.
- 659 Huang, D. D., Zhang, Q., Cheung, H. H. Y., Yu, L., Zhou, S., Anastasio, C., Smith, J. D., and  
660 Chan, C. K.: Formation and Evolution of aqSOA from Aqueous-Phase Reactions of  
661 Phenolic Carbonyls: Comparison between Ammonium Sulfate and Ammonium Nitrate  
662 Solutions, *Environ. Sci. Technol.*, 52, 9215–9224, <https://doi.org/10.1021/acs.est.8b03441>,  
663 2018.
- 664 Huang, R. J., Zhang, Y., Bozzetti, C., Ho, K. F., Cao, J. J., Han, Y., Daellenbach, K. R., Slowik,  
665 J. G., Platt, S. M., Canonaco, F., Zotter, P., Wolf, R., Pieber, S. M., Bruns, E. A., Crippa,  
666 M., Ciarelli, G., Piazzalunga, A., Schwikowski, M., Abbaszade, G., Schnelle-Kreis, J.,  
667 Zimmermann, R., An, Z., Szidat, S., Baltensperger, U., El Haddad, I., and Prévôt, A. S. H.:  
668 High secondary aerosol contribution to particulate pollution during haze events in China,  
669 *Nature*, 514, 218–222, <https://doi.org/10.1038/nature13774>, 2014.
- 670 Huang, R. J., Wang, Y., Cao, J., Lin, C., Duan, J., Chen, Q., Li, Y., Gu, Y., Yan, J., Xu, W.,  
671 Fröhlich, R., Canonaco, F., Bozzetti, C., Ovadnevaite, J., Ceburnis, D., Canagaratna, M. R.,  
672 Jayne, J., Worsnop, D. R., El-Haddad, I., Prevot, A. S. H., and O’Dowd, C. D.: Primary

- 673 emissions versus secondary formation of fine particulate matter in the most polluted city  
674 (Shijiazhuang) in North China, *Atmos. Chem. Phys.*, 19, 2283–2298,  
675 <https://doi.org/10.5194/acp-19-2283-2019>, 2019.
- 676 Huang, R. J., He, Y., Duan, J., Li, Y., Chen, Q., Zheng, Y., Chen, Y., Hu, W., Lin, C., Ni, H.,  
677 Dai, W., Cao, J., Wu, Y., Zhang, R., Xu, W., Ovadnevaite, J., Ceburnis, D., Hoffmann, T.,  
678 and D. O'Dowd, C.: Contrasting sources and processes of particulate species in haze days  
679 with low and high relative humidity in wintertime Beijing, *Atmos. Chem. Phys.*, 20, 9101–  
680 9114, <https://doi.org/10.5194/acp-20-9101-2020>, 2020.
- 681 Jimenez, J. L., Jayne, J. T., Shi, Q., Kolb, C. E., Worsnop, D. R., Yourshaw, I., Seinfeld, J. H.,  
682 Flagan, R. C., Zhang, X., Smith, K. A., Morris, J. W., and Davidovits, P.: Ambient aerosol  
683 sampling using the Aerodyne aerosol mass spectrometer, *J. Geophys. Res. Atmos.*, 108, 1–  
684 13, <https://doi.org/10.1029/2001jd001213>, 2003.
- 685 Jimenez, J. L., Canagaratna, M. R., Donahue, N. M., Prevot, A. S. H., Zhang, Q., Kroll, J. H.,  
686 DeCarlo, P. F., Allan, J. D., Coe, H., Ng, N. L., Aiken, A. C., Docherty, K. S., Ulbrich, I.  
687 M., Grieshop, A. P., Robinson, A. L., Duplissy, J., Smith, J. D., Wilson, K. R., Lanz, V. A.,  
688 Hueglin, C., Sun, Y. L., Tian, J., Laaksonen, A., Raatikainen, T., Rautiainen, J., Vaattovaara,  
689 P., Ehn, M., Kulmala, M., Tomlinson, J. M., Collins, D. R., Cubison, M. J., Dunlea, E. J.,  
690 Huffman, J. A., Onasch, T. B., Alfarra, M. R., Williams, P. I., Bower, K., Kondo, Y.,  
691 Schneider, J., Drewnick, F., Borrmann, S., Weimer, S., Demerjian, K., Salcedo, D., Cottrell,  
692 L., Griffin, R., Takami, A., Miyoshi, T., Hatakeyama, S., Shimono, A., Sun, J. Y., Zhang,  
693 Y. M., Dzepina, K., Kimmel, J. R., Sueper, D., Jayne, J. T., Herndon, S. C., Trimborn, A.  
694 M., Williams, L. R., Wood, E. C., Middlebrook, A. M., Kolb, C. E., Baltensperger, U., and  
695 Worsnop, D. R.: Evolution of organic aerosols in the atmosphere, *Science (80- )*, 326,  
696 1525–1529, <https://doi.org/10.1126/science.1180353>, 2009.
- 697 Kuang, Y., He, Y., Xu, W., Yuan, B., Zhang, G., Ma, Z., Wu, C., Wang, C., Wang, S., Zhang,  
698 S., Tao, J., Ma, N., Su, H., Cheng, Y., Shao, M., and Sun, Y.: Photochemical Aqueous-Phase  
699 Reactions Induce Rapid Daytime Formation of Oxygenated Organic Aerosol on the North  
700 China Plain, *Environ. Sci. Technol.*, 54, 3849–3860,  
701 <https://doi.org/10.1021/acs.est.9b06836>, 2020.
- 702 Lee, A. K. Y., Chen, C. L., Liu, J., Price, D. J., Betha, R., Russell, L. M., Zhang, X., and Cappa,  
703 C. D.: Formation of secondary organic aerosol coating on black carbon particles near  
704 vehicular emissions, *Atmos. Chem. Phys.*, 17, 15055–15067, <https://doi.org/10.5194/acp-17-15055-2017>, 2017.
- 706 Li, H., Zhang, Q., Zhang, Q., Chen, C., Wang, L., Wei, Z., Zhou, S., Parworth, C., Zheng, B.,  
707 Canonaco, F., Prévôt, A. S. H., Chen, P., Zhang, H., Wallington, T. J., and He, K.:  
708 Wintertime aerosol chemistry and haze evolution in an extremely polluted city of the North  
709 China Plain: Significant contribution from coal and biomass combustion, *Atmos. Chem.  
710 Phys.*, 17, 4751–4768, <https://doi.org/10.5194/acp-17-4751-2017>, 2017.

- 711 Li, J., Liu, Z., Gao, W., Tang, G., Hu, B., Ma, Z., and Wang, Y.: Insight into the formation and  
712 evolution of secondary organic aerosol in the megacity of Beijing, China, *Atmos. Environ.*,  
713 220, <https://doi.org/10.1016/j.atmosenv.2019.117070>, 2020.
- 714 Middlebrook, A. M., Bahreini, R., Jimenez, J. L., and Canagaratna, M. R.: Evaluation of  
715 composition-dependent collection efficiencies for the Aerodyne aerosol mass spectrometer  
716 using field data, *Aerosol Sci. Technol.*, 46, 258–271,  
717 <https://doi.org/10.1080/02786826.2011.620041>, 2012.
- 718 Ng, N. L., Canagaratna, M. R., Zhang, Q., Jimenez, J. L., Tian, J., Ulbrich, I. M., Kroll, J. H.,  
719 Docherty, K. S., Chhabra, P. S., Bahreini, R., Murphy, S. M., Seinfeld, J. H., Hildebrandt,  
720 L., Donahue, N. M., Decarlo, P. F., Lanz, V. A., Prévôt, A. S. H., Dinar, E., Rudich, Y., and  
721 Worsnop, D. R.: Organic aerosol components observed in Northern Hemispheric datasets  
722 from Aerosol Mass Spectrometry, *Atmos. Chem. Phys.*, 10, 4625–4641,  
723 <https://doi.org/10.5194/acp-10-4625-2010>, 2010.
- 724 Ng, N. L., Canagaratna, M. R., Jimenez, J. L., Chhabra, P. S., Seinfeld, J. H., and Worsnop, D.  
725 R.: Changes in organic aerosol composition with aging inferred from aerosol mass spectra,  
726 *Atmos. Chem. Phys.*, 11, 6465–6474, <https://doi.org/10.5194/acp-11-6465-2011>, 2011.
- 727 Onasch, T. B., Trimborn, A., Fortner, E. C., Jayne, J. T., Kok, G. L., Williams, L. R., Davidovits,  
728 P., and Worsnop, D. R.: Soot particle aerosol mass spectrometer: Development, validation,  
729 and initial application, *Aerosol Sci. Technol.*, 46, 804–817,  
730 <https://doi.org/10.1080/02786826.2012.663948>, 2012.
- 731 Paatero, P.: The Multilinear Engine—A Table-Driven, Least Squares Program for Solving  
732 Multilinear Problems, Including the n-Way Parallel Factor Analysis Model, *J. Comput.*  
733 *Graph. Stat.*, 8, 854–888, <https://doi.org/10.1080/10618600.1999.10474853>, 1999.
- 734 Sullivan, A. P., Hodas, N., Turpin, B. J., Skog, K., Keutsch, F. N., Gilardoni, S., Paglione, M.,  
735 Rinaldi, M., Decesari, S., Cristina Facchini, M., Poulain, L., Herrmann, H., Wiedensohler,  
736 A., Nemitz, E., Twigg, M., and Collett, J. L.: Evidence for ambient dark aqueous SOA  
737 formation in the Po Valley, Italy, *Atmos. Chem. Phys.*, 16, 8095–8108,  
738 <https://doi.org/10.5194/acp-16-8095-2016>, 2016.
- 739 Sun, Y., Chen, C., Zhang, Y., Xu, W., Zhou, L., Cheng, X., Zheng, H., Ji, D., Li, J., Tang, X.,  
740 Fu, P., and Wang, Z.: Rapid formation and evolution of an extreme haze episode in Northern  
741 China during winter 2015, 1–9, <https://doi.org/10.1038/srep27151>, 2016.
- 742 Sun, Y., Xu, W., Zhang, Q., Jiang, Q., Canonaco, F., Prévôt, A. S. H., Fu, P., Li, J., Jayne, J.,  
743 Worsnop, D. R., and Wang, Z.: Source apportionment of organic aerosol from 2-year highly  
744 time-resolved measurements by an aerosol chemical speciation monitor in Beijing, China,  
745 *Atmos. Chem. Phys.*, 18, 8469–8489, <https://doi.org/10.5194/acp-18-8469-2018>, 2018a.
- 746 Sun, Y., Xu, W., Zhang, Q., Jiang, Q., Canonaco, F., and Prévôt, A. S. H.: Source  
747 apportionment of organic aerosol from two-year highly time- resolved measurements by an  
748 aerosol chemical speciation monitor in Beijing , China, 2018b.



- 749 Sun, Y. L., Zhang, Q., Anastasio, C., and Sun, J.: Insights into secondary organic aerosol  
750 formed via aqueous-phase reactions of phenolic compounds based on high resolution mass  
751 spectrometry, *Atmos. Chem. Phys.*, 10, 4809–4822, [https://doi.org/10.5194/acp-10-4809-](https://doi.org/10.5194/acp-10-4809-2010)  
752 2010, 2010.
- 753 Wang, J., Ye, J., Zhang, Q., Zhao, J., Wu, Y., Li, J., Liu, D., Li, W., Zhang, Y., Wu, C., Xie,  
754 C., Qin, Y., Lei, Y., Huang, X., Guo, J., Liu, P., Fu, P., Li, Y., Lee, H. C., Choi, H., Zhang,  
755 J., Liao, H., Chen, M., Sun, Y., Ge, X., Martin, S. T., and Jacob, D. J.: Aqueous production  
756 of secondary organic aerosol from fossil-fuel emissions in winter Beijing haze, *Proc. Natl.*  
757 *Acad. Sci. U. S. A.*, 118, 1–6, <https://doi.org/10.1073/pnas.2022179118>, 2021.
- 758 Wang, S., Newland, M. J., Deng, W., Rickard, A. R., Hamilton, J. F., Muñoz, A., Ródenas, M.,  
759 Vázquez, M. M., Wang, L., and Wang, X.: Aromatic Photo-oxidation, A New Source of  
760 Atmospheric Acidity, *Environ. Sci. Technol.*, 54, 7798–7806,  
761 <https://doi.org/10.1021/acs.est.0c00526>, 2020.
- 762 Xu, S., Liu, W., and Tao, S.: Emission of Polycyclic Aromatic Hydrocarbons in China,  
763 *Biophys. Process. Anthropol. Org. Compd. Environ. Syst.*, 40, 267–281,  
764 <https://doi.org/10.1002/9780470944479.ch11>, 2006.
- 765 Xu, W., Han, T., Du, W., Wang, Q., Chen, C., Zhao, J., Li, J., Fu, P., Wang, Z., Worsnop, D.  
766 R., and Sun, Y.: Effects of Aqueous-phase and Photochemical Processing on Secondary  
767 Organic Aerosol Formation and Evolution in Beijing, China,  
768 <https://doi.org/10.1021/acs.est.6b04498>, 2017.
- 769 Xu, W., Sun, Y., Wang, Q., Zhao, J., Wang, J., Ge, X., Xie, C., Zhou, W., Du, W., Li, J., Fu,  
770 P., Wang, Z., Worsnop, D. R., and Coe, H.: Changes in Aerosol Chemistry From 2014 to  
771 2016 in Winter in Beijing: Insights From High-Resolution Aerosol Mass Spectrometry, *J.*  
772 *Geophys. Res. Atmos.*, 124, 1132–1147, <https://doi.org/10.1029/2018JD029245>, 2019.
- 773 Ye, C., Liu, P., Ma, Z., Xue, C., Zhang, C., Zhang, Y., Liu, J., Liu, C., Sun, X., and Mu, Y.:  
774 High H<sub>2</sub>O<sub>2</sub> Concentrations Observed during Haze Periods during the Winter in Beijing:  
775 Importance of H<sub>2</sub>O<sub>2</sub> Oxidation in Sulfate Formation, *Environ. Sci. Technol. Lett.*, 5, 757–  
776 763, <https://doi.org/10.1021/acs.estlett.8b00579>, 2018.
- 777 Zhang, Q., Jimenez, J. L., Canagaratna, M. R., Ulbrich, I. M., Ng, N. L., Worsnop, D. R., and  
778 Sun, Y.: Understanding atmospheric organic aerosols via factor analysis of aerosol mass  
779 spectrometry: A review, <https://doi.org/10.1007/s00216-011-5355-y>, 2011.
- 780 Zhao, J., Qiu, Y., Zhou, W., Xu, W., Wang, J., Zhang, Y., Li, L., Xie, C., Wang, Q., Du, W.,  
781 Worsnop, D. R., Canagaratna, M. R., Zhou, L., Ge, X., Fu, P., Li, J., Wang, Z., Donahue, N.  
782 M., and Sun, Y.: Organic Aerosol Processing During Winter Severe Haze Episodes in  
783 Beijing, *J. Geophys. Res. Atmos.*, 124, 10248–10263,  
784 <https://doi.org/10.1029/2019JD030832>, 2019.

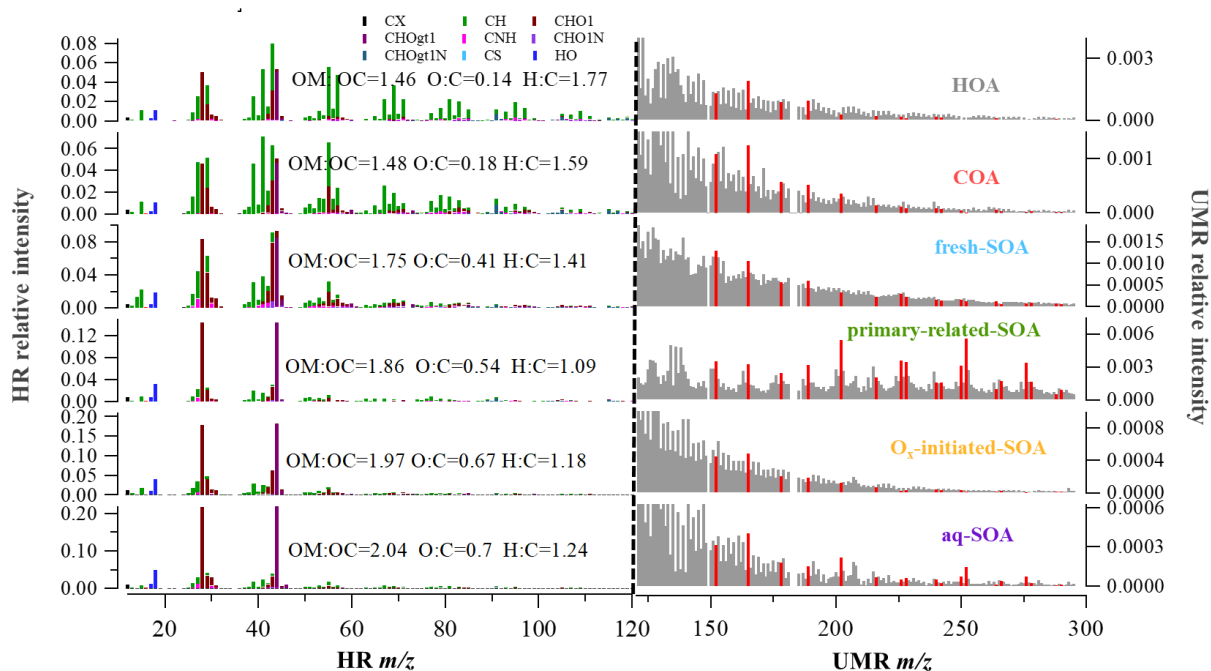
785

786

787

788

789 **Figures**

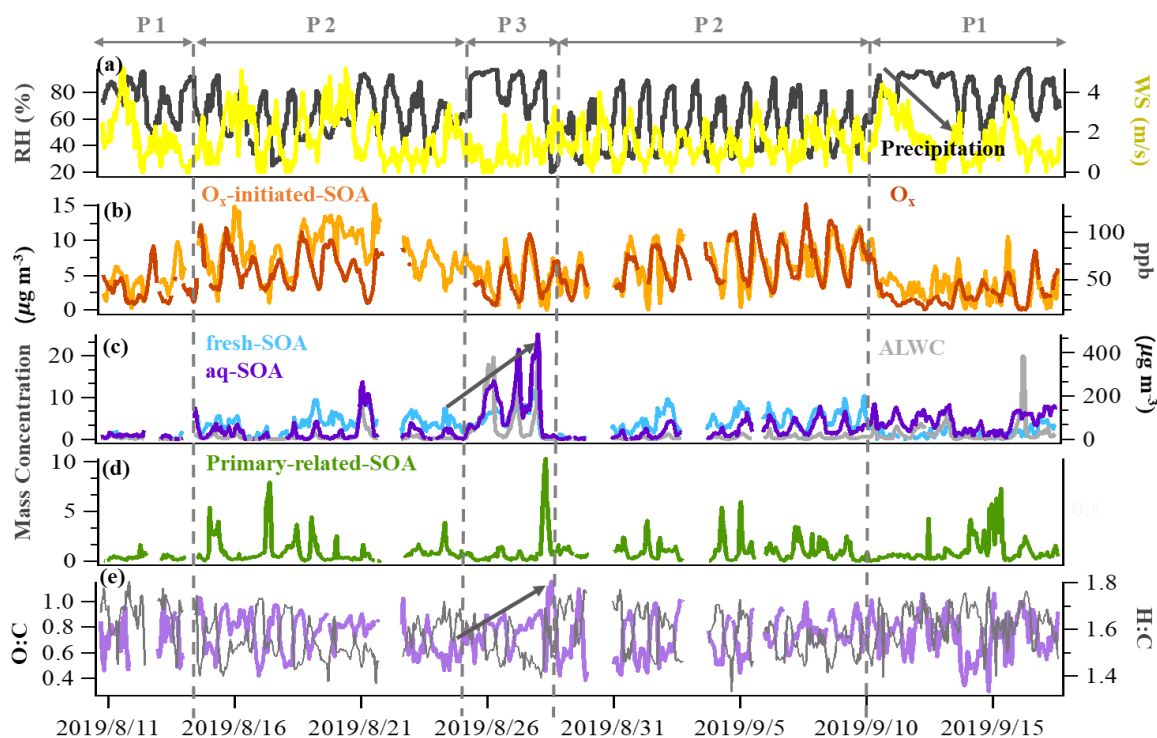


790

791 **Fig. 1** HR and UMR mass spectra of OA factors: (a) HOA; (b) COA; (c) fresh-SOA; (d)  
792 primary-related-SOA; (e) ~~phochem-SOA~~  $O_x$ -initiated-SOA; (f) aq-SOA. Mass spectra signals  
793 less than 120 amu are colored by nine ion categories, signals equal to or greater than 120 amu  
794 are in unit mass resolution, and polycyclic aromatic hydrocarbons (PAHs) signals are in red on  
795 the right panels.

796

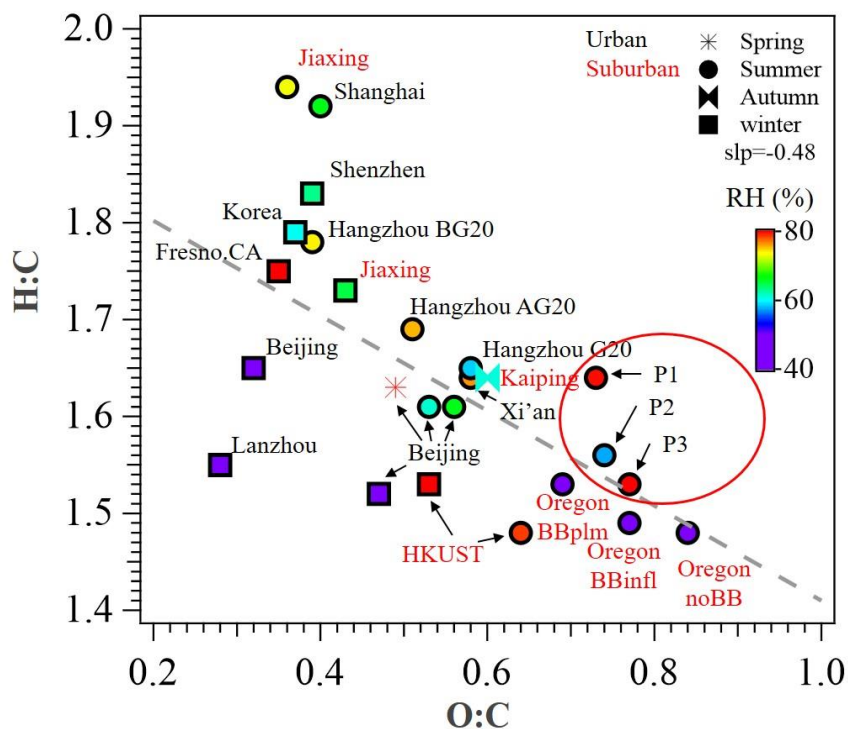
797



798

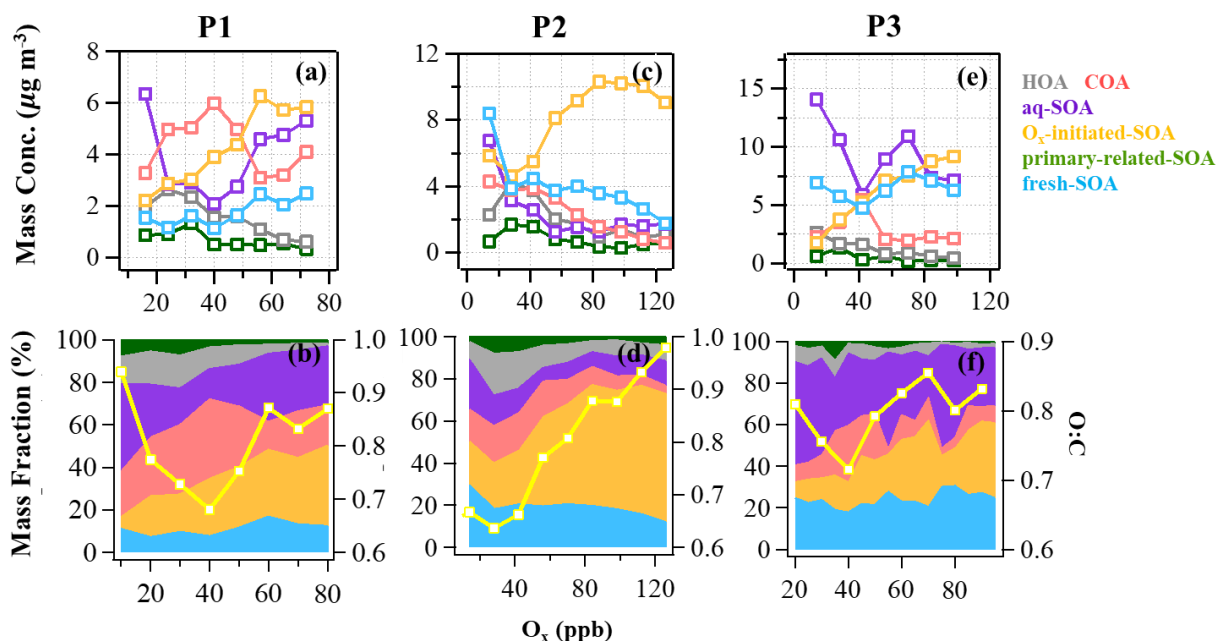
799 **Fig. 2** Time series of (a) relative humidity (RH) and wind speed (WS), (b) O<sub>x</sub> and ~~photochem-~~  
 800 ~~SOA~~O<sub>x</sub>-initiated-SOA, (c) fresh-SOA, aq-SOA and ALWC, (d) primary-related-SOA, (e) the  
 801 O:C ratio and H:C ratio. The time series were categorized to be three typical periods based on  
 802 total SOA mass concentrations and meteorology conditions: reference period (P1), high O<sub>x</sub>  
 803 period (P2) and high RH period (P3).

804



805

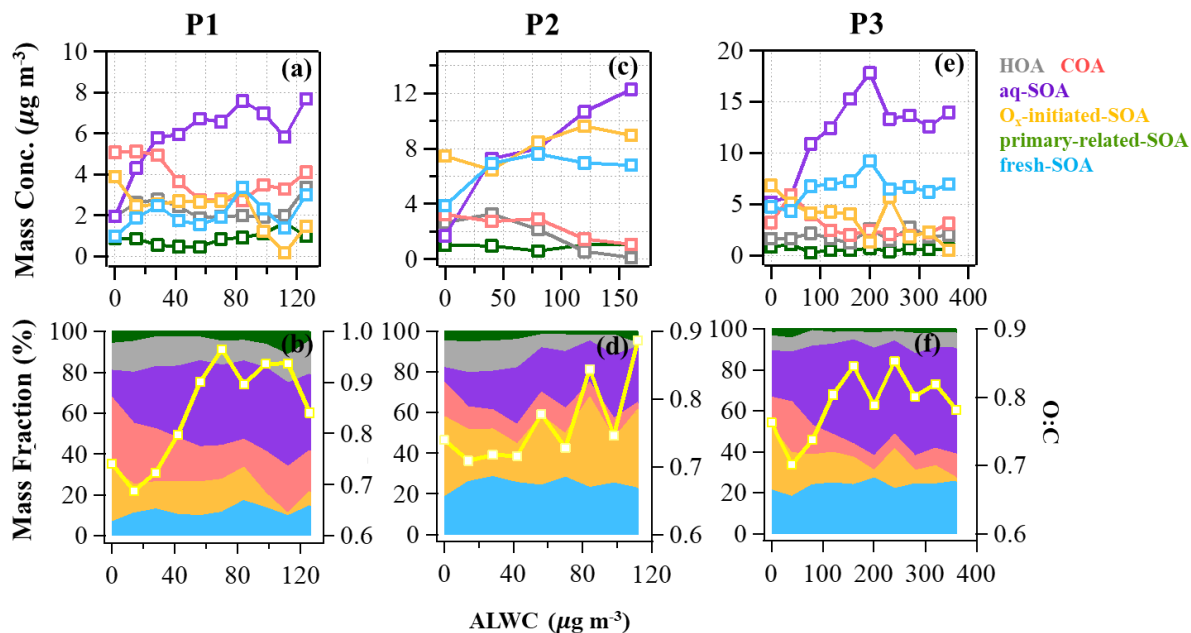
806 **Fig.3** Van Krevelen plot for OA of urban and suburban sites in China and other nations. Data  
 807 points are colored by RH (%). P1, P2 and P3 in red circles represents the different periods in  
 808 this study. All the data and related references can be found in Table S3.



809

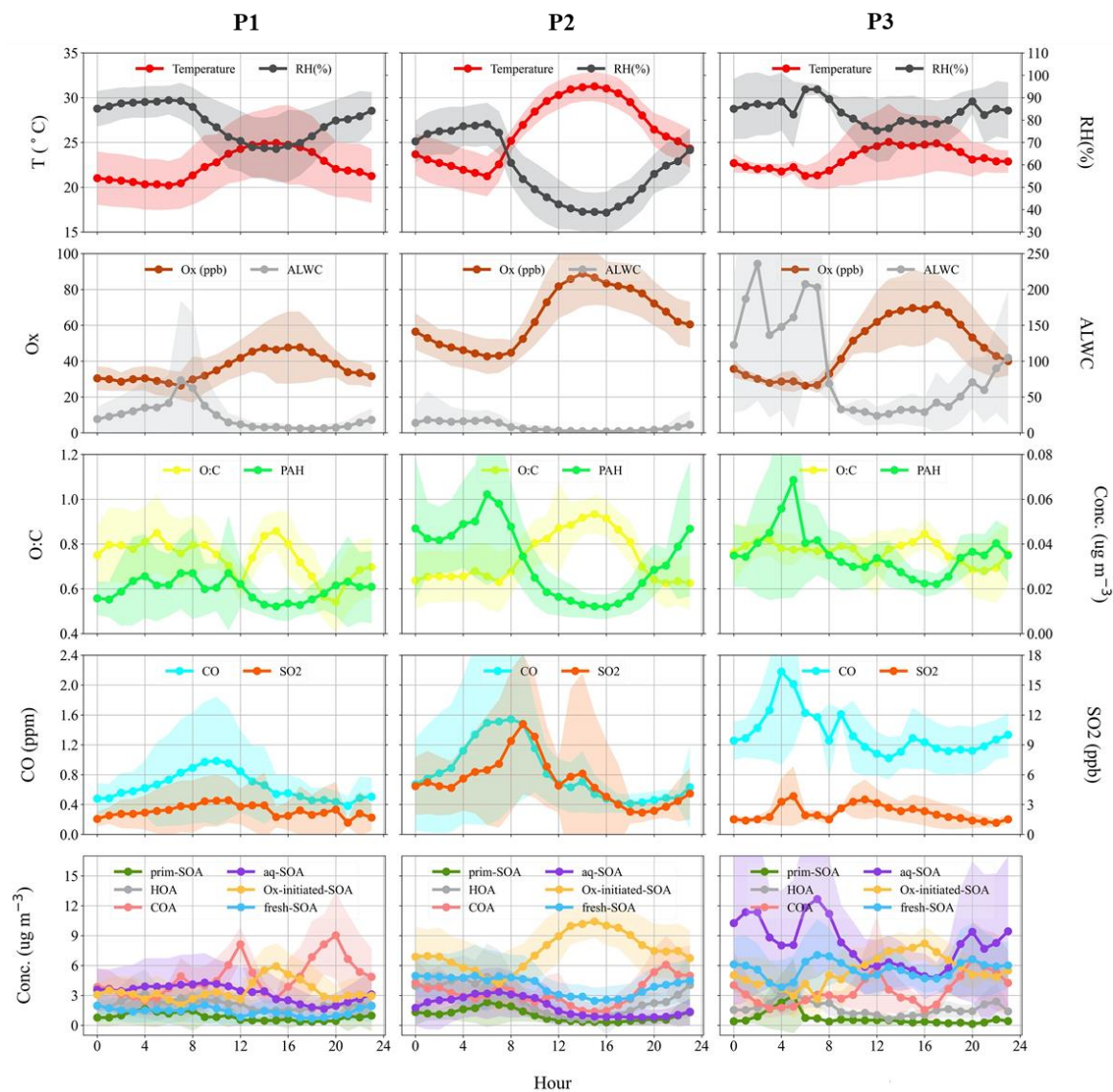
810 **Fig. 4** The mass concentration and contribution of OA factors as functions of  $O_x$  in reference  
 811 period (P1: a & b), high  $O_x$  period (P2: c & d) and high RH period (P3: e & f) during this

812 campaign. The yellow curves represent the O:C ratio vs.  $O_x$ . The data were binned according  
 813 to  $O_x$  concentration (10 ppb increment in P1, 20 ppb increment in P2 and P3).



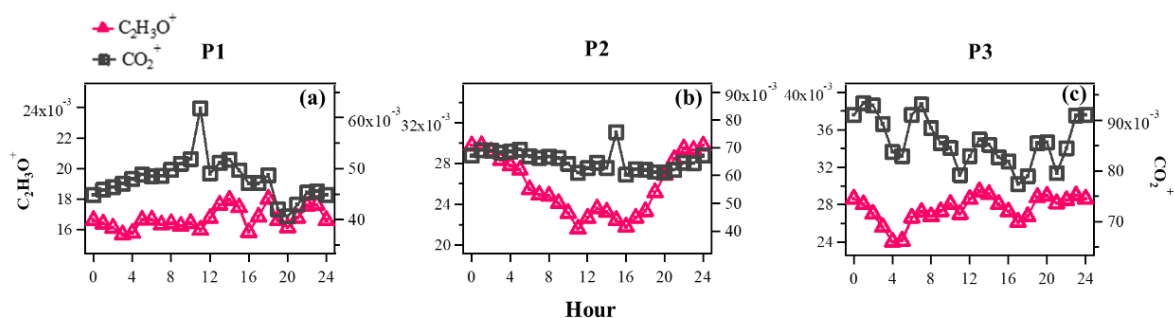
814

815 **Fig. 5** The mass concentration and contribution of OA factors as functions of ALWC in  
 816 reference period (P1: a & b), high  $O_x$  period (P2: c & d) and high RH period (P3: e & f) during  
 817 this campaign. The yellow curves represent the O:C ratio v.s. ALWC. The data were binned  
 818 according to the ALWC concentration ( $20 \mu\text{g m}^{-3}$  increment in P1 and P2,  $50 \mu\text{g m}^{-3}$  increment  
 819 in P3).



820

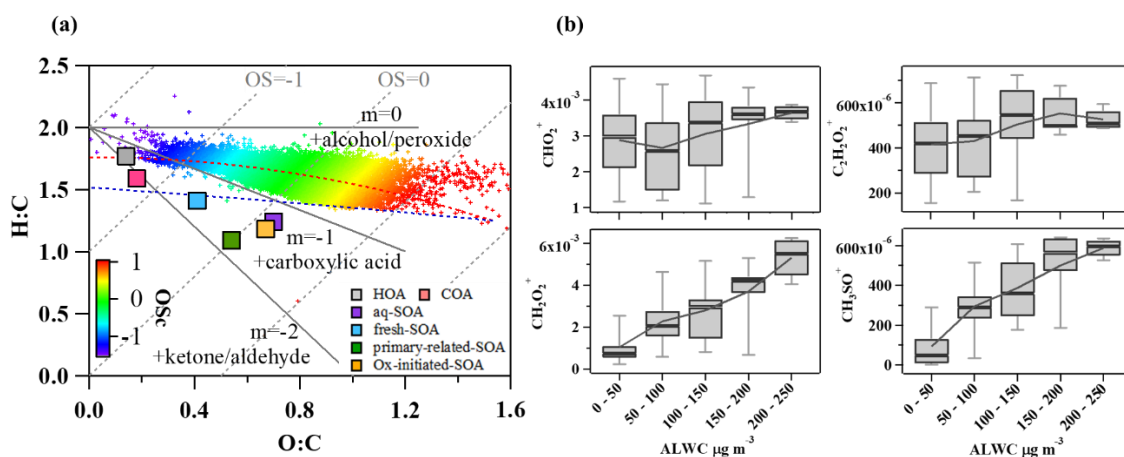
821 **Fig. 6** Diurnal patterns of meteorological parameters (T, RH), gaseous species (O<sub>x</sub>, CO, SO<sub>2</sub>),  
 822 ALWC (liquid water content), O:C (oxygen-to-carbon elemental ratio), polycyclic aromatic  
 823 hydrocarbons (PAHs) fragments and OA factors in reference period (P1), high O<sub>x</sub> period (P2)  
 824 and high RH period (P3) in this campaign.



825

826 **Fig. 7** Evolution of high-resolution organic mass spectra on changes in relative intensities (mass  
 827 fraction) of oxygen-containing ions:  $C_2H_3O^+$  ( $m/z$  43) and  $CO_2^+$  ( $m/z$  44) in reference period  
 828 (P1:a), high  $O_x$  period (P2: b) and high RH period (P3: c) in this campaign.

829



830

831 **Fig. 8** (a) Van Krevelen diagram for the O:C and H:C ratios of different OA factors (marked  
 832 with squares) and bulk of OA during summer (marked with plus signs and colored by  
 833 Oscarbon oxidation state (OSc)); (b) Mass fractions of ion fragments indicative of aqueous-  
 834 phase processing and oxygenated functional groups (alcohols, carboxylic acids) as a function  
 835 of ALWC.